

# Learning to See and Act: Task-Aware Virtual View Exploration for Robotic Manipulation

Yongjie Bai<sup>1,2,\*</sup> Zhouxia Wang<sup>1,3,\*</sup> Yang Liu<sup>1,✉</sup> Kaijun Luo<sup>1</sup> Yifan Wen<sup>1</sup> Mingtong Dai<sup>2,4</sup>  
 Weixing Chen<sup>1</sup> Ziliang Chen<sup>2</sup> Lingbo Liu<sup>2</sup> Guanbin Li<sup>1,2</sup> Liang Lin<sup>1,2,5</sup>

<sup>1</sup>Sun Yat-sen University <sup>2</sup>Pengcheng Laboratory <sup>3</sup>Nanyang Technological University

<sup>4</sup>Shenzhen Institutes of Advanced Technology, Chinese Academy of Sciences <sup>5</sup>X-Era AI Lab

## Abstract

Recent vision-language-action (VLA) models for multi-task robot manipulation often rely on fixed camera setups and shared visual encoders, which limit their performance under occlusions and during cross-task transfer. To address these challenges, we propose **Task-aware Virtual View Exploration (TVVE)**, a framework that learns to select task-relevant virtual camera viewpoints and dynamically re-render observations from a reconstructed scene representation using the selected viewpoints. To enable efficient view selection, we train an exploration policy in a pseudo-environment. In addition, we introduce a **Task-aware Mixture-of-Experts (TaskMoE)** visual encoder that routes visual features to task-specialized experts, mitigating interference in multi-task learning. To evaluate robustness under distribution shifts, we construct **RLBench-OG**, an out-of-distribution benchmark with visual perturbations and camera pose variations. Experiments on RLBench and RLBench-OG demonstrate that TVVE achieves higher success rates than strong baselines, while real-robot experiments further confirm its robustness to visual disturbances and unseen instructions. Code and visualizations are available at: [TAVP](#).

## 1. Introduction

A general-purpose robotic system is expected to accurately perform numerous manipulation tasks [32]. With the development of vision-language-action (VLA) models [2–7, 27–31, 47] and transformer-based architectures [2, 3, 9, 20, 57], many end-to-end robotic manipulation frameworks (e.g., OpenVLA[27],  $\pi_0$ [1]) have achieved promising results on complex and fine-grained tasks. Typically, these models rely on observations captured from a single view [9, 27, 44]

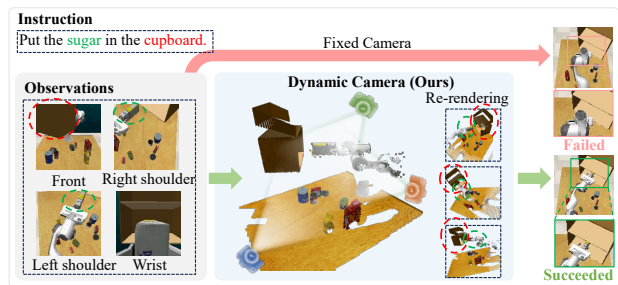


Figure 1. **Motivation Illustration.** Observations captured from fixed cameras often miss parts of the target objects. For example, the front view only captures the cupboard (highlighted with a red circles), while the left and right shoulder views only show the sugar (already grasped by the end-effector and highlighted with green circles). These incomplete observations may lead to failed operations. In contrast, our proposed TVVE is designed to dynamically explore and re-render informative viewpoints that maximize coverage of target-relevant information, thereby improving the reliability of manipulation outcomes.

or a few fixed viewpoints [24, 45] to guide action prediction. While this may suffice in simple environments with only a few objects, it becomes problematic in cluttered or dynamic scenes—particularly when objects or the end-effector are repositioned during task execution.

In such scenarios, fixed viewpoints often lead to occlusions of the target object or the end-effector, resulting in incomplete scene understanding and inaccurate action predictions. As shown in Fig. 1, given the instruction “Put the sugar in the cupboard”, images captured from three fixed cameras either miss the cupboard or fail to include the end-effector grasped with sugar. Such incomplete visual observations prevent the robot from correctly interpreting the scene, ultimately leading to suboptimal or failed actions.

Beyond acquiring complete and informative visual features, a scalable and task-sensitive visual encoder is also critical for accurate perception in multi-task settings. Although prior language-conditioned transformer-based methods, such as RVT [15] and RVT-2 [16], enable

\* Equal Contribution ✉ Corresponding author  
 Accepted by CVPR 2026

multi-task capabilities by attending to instruction tokens, their shared encoders still suffer from task interference, especially when handling visually and semantically diverse tasks (e.g., *pick an apple* vs. *open a drawer*). This entanglement limits the generalization and scalability of such models across a broad range of manipulation behaviors.

To address these challenges, we propose the **Task-aware Virtual View Exploration (TVVE)** model, which integrates viewpoint exploration with task-aware visual feature extraction for robust and generalizable multi-task robotic manipulation. TVVE explores informative viewpoints using a delicately designed efficient reinforcement learning-based exploration policy, while employing a scalable task-aware Mixture-of-Experts (MoE) visual encoder to extract task-specific features. This design enables the model to obtain more complete and discriminative visual information, thereby improving robustness and generalization in multi-task action prediction.

Specifically, our task-aware Mixture-of-Experts module, termed **TaskMoE**, improves multi-task accuracy and generalization through two key designs: (1) a dynamic expert routing mechanism guided by fused instruction and scene cues, rather than relying solely on task identifiers; and (2) a decoupled gating strategy that enables parameter sharing among semantically similar tasks, while isolating routing for semantically diverse ones. Based on the extracted task-specific features, we introduce the Multi-Viewpoint Exploration Policy (MVPEP) that adaptively selects task-specific camera poses based on the global point cloud. By re-rendering 2D observations from the explored viewpoints, MVPEP enriches visual perception with globally aware features, leading to more informed action prediction and improved manipulation success.

To comprehensively evaluate the effectiveness of our TVVE in enhancing robotic spatial understanding and action generation performance, as well as its multi-task perception and decision-making capabilities, we conducted rigorous benchmark testing on 18 diverse RL-Bench [22] simulation tasks covering multiple tasks and scenarios. Our contributions are summarized as follows:

- **Multi-Viewpoint Exploration Policy (MVPEP)** : The MVPEP enables robots to explore better virtual observation viewpoints (dynamic multi-view re-rendering), effectively addressing occlusion and insufficient viewpoint problems, and enhancing 3D perception capabilities.
- **Task-aware Mixture-of-Experts (TaskMoE)**: We introduce TaskMoE, which dynamically selects perception and action generation experts according to the task and its related instruction and scene visual information, improving multi-task processing capability and robustness.
- **RL-Bench-OG**: We construct a new benchmark to comprehensively evaluate the model robustness and generalization under out-of-distribution (OOD) settings, cover-

ing visual perturbations such as occlusions, background changes, lighting variations, texture shifts, and camera pose changes.

- **Superior Robotic Manipulation Performance**: Extensive experiments on RL-Bench, RL-Bench-OG and real-robot tasks demonstrate that our TVVE significantly outperforms existing baselines in multi-task manipulation w.r.t accuracy and robustness.

## 2. Related Works

### 2.1. Multi-task Learning in Manipulation

The core challenges for general-purpose robots lie in task generalization capabilities and multi-task execution in complex environments. In the past, multi-task learning [11, 16, 35, 52] has achieved remarkable progress. It primarily consists of two approaches: Modular solutions decompose skills into reusable basic units (e.g., perception, planning, and control modules) [36]. Though interpretable, they face the combinatorial explosion problem—as task complexity increases, the cost of designing interfaces and coordinating between modules grows exponentially, leading to system rigidity. For instance, ManipGen [10] consumed massive training resources to train over 1,000 task-specific experts. Conversely, end-to-end solutions employ a single dense model to directly map perception to action [9, 19, 37, 44, 47, 49, 53]. While simplifying the pipeline, significant differences in visual feature distributions and motion patterns across tasks (e.g., grasping fragile objects vs. tightening screws) cause the model to struggle with convergence during training due to parameter conflicts. The Mixture of Experts (MoE) [43] addresses the scaling bottleneck of large models through a sparse activation mechanism. SDP [50] integrated MoE into diffusion policies to address multi-task learning and task transfer. Differently, we propose a task-aware MoE (TaskMoE) to resolve feature conflicts between different robotic manipulation tasks, activating distinct task-specific experts for different tasks, thereby enhancing multi-task execution performance and generalization capabilities.

### 2.2. Vision-Language-Action Model

Recently, numerous VLA models [16, 44, 47, 53, 55] have been proposed. In contrast to traditional pipelines that rely on explicit pose estimation [12, 13] and path planning [39, 56], VLA models directly map linguistic instructions and visual observations to low-level actions, substantially simplifying the control stack. With the advancement of large language models (LLMs) and vision-language models (VLMs), these large models have been applied in robotics [2–4, 7, 27, 29], leveraging their powerful priors to provide world knowledge for robots, thereby enhancing model generalization and performance. However, most ex-

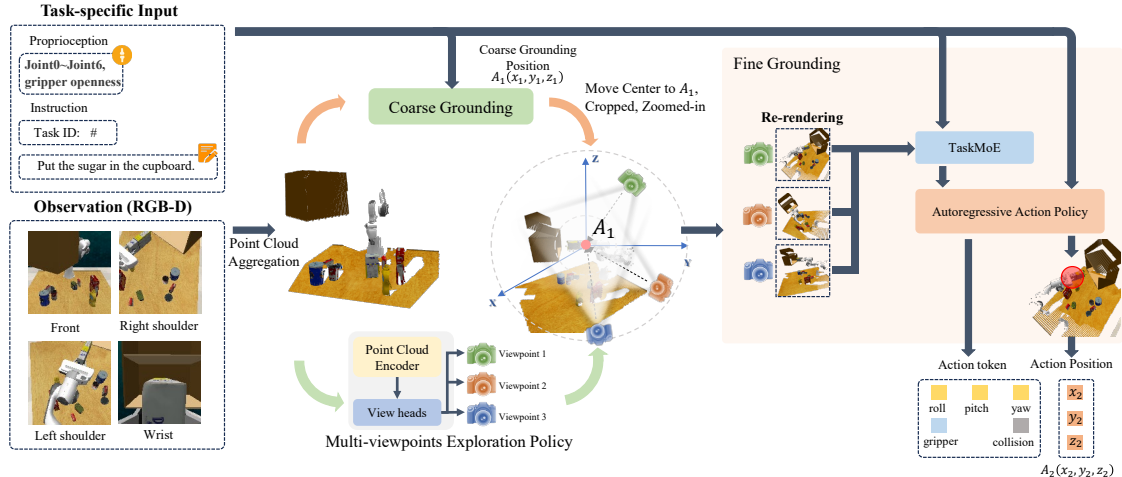


Figure 2. The overview of our Task-aware Virtual View Exploration (TVVE) framework. The input of this framework is multiple RGB-D images from fixed viewpoints. First, it converts them into point clouds and aggregates them into a global point cloud in the world coordinate system. Then, it diverges into two branches: One branch (orange) performs **Coarse Grounding** to predict the approximate position of the end-effector. Subsequently, it moves the center of the global point cloud to this predicted position, performs scaling and cropping, retaining the important point cloud region. Another branch (green) receives the global point cloud, passes it through MVEP to predict the optimal camera parameters for the observation viewpoint. Then, using these parameters, it renders a 2D image from the point cloud processed by the red branch. This rendered image is fed into the **Fine Grounding** to predict the final robot action, including the end-effector position, rotation, gripper status, and collision state.

isting VLA models operate on a single or fixed viewpoint, limiting a robot’s ability to form comprehensive 3D spatial understanding and thereby constraining action prediction. To overcome this limitation, we introduce a dynamic multi-view re-rendering perception scheme that enhances spatial perception and scene comprehension, ultimately improving execution robustness in complex environments.

### 2.3. Reinforcement Learning in Robotics

Reinforcement learning (RL) has achieved significant accomplishments in robotics [46]. However, implementing RL starting from scratch typically necessitates complex reward mechanism and training paradigm design [21, 26, 34, 41, 48]. Recently, several works [18, 33] have demonstrated promising results by using RL to fine-tune pre-trained models. To optimize our MVEP (Multi-Viewpoint Exploration Policy), we designed pseudo-environment interactions and a view-aware reward function, enabling policy learning based on a pre-trained model using offline expert data. Furthermore, to adapt between the MVEP and the action policy, we introduce supervised post-training to coordinate the robot’s ability to “See and Act”, thereby enhancing its task execution performance.

## 3. Methodology

### 3.1. Overview

Our proposed **Task-aware Virtual View Exploration (TVVE)** framework aims to identify better viewpoints for accurate and robust robotic manipulation, guided by task-specific visual feature extraction. The full pipeline is illus-

trated in Fig. 2. TVVE takes as input a language instruction, the current visual observations from RGB-D cameras, and the current gripper state. To enable the model to explore the better observations from arbitrary viewpoints, we first reconstruct a 3D point cloud of the scene using the input RGB-D images. To narrow down the search space and enable task-aligned view selection, we leverage the coarse prediction stage from RVT-2 [16] to generate an area of interest. However, unlike RVT-2, which extracts visual features for all tasks using a shared Multi-View Transformer (MVT), we integrate a **Task-Aware Mixture-of-Experts (TaskMoE)** module within the MVT to route instructions to specialized expert encoders. This design enables more precise and task-aligned visual feature extraction, which benefits both viewpoint selection and action prediction. Starting from the identified area of interest, we employ a **Multi-Viewpoint Exploration Policy (MVEP)** to search for better camera poses that maximize the visibility of the target object and the end-effector. The selected viewpoints are then re-rendered into image observations and processed using another TaskMoE-based MVT before being passed to the action prediction model. For action prediction, we also upgrade the autoregressive action policy proposed in ARP [55] with our proposed TaskMoE to attain more task-specific feature extraction and action prediction.

In the following sections, we detail the design of: 1) the TaskMoE, 2) the MVEP, and 3) the training strategy.

### 3.2. TaskMoE

To address the inherent heterogeneity of complex manipulation tasks in multi-task learning, where different tasks often require substantially distinct visual representations and action policies, we introduce a task-aware Mixture-of-Experts module (TaskMoE), as illustrated in Fig. 3. Compared to prior MoE-based approaches [43, 50], our TaskMoE introduces two key innovations.

First, instead of relying solely on task identifiers for expert selection, we incorporate richer instruction- and scene-related cues to guide expert routing more effectively, which is crucial for accurate multi-task robotic manipulation. Specifically, as shown in Fig. 3, we design a cross-modality module that employs a cross-attention mechanism to model the interaction between instruction and visual information. The resulting context-aware features are then fused with the task identifier via a Feature-wise Linear Modulation (FiLM) layer [38], enabling more adaptive and task-sensitive expert selection.

Second, to improve the scalability and generalization of TaskMoE, we decouple the number of routing gates from the total number of tasks. Concretely, we allocate  $N_G$  gates for all  $N_J$  tasks, where  $N_G < N_J$ . This design not only accommodates task diversity but also promotes parameter sharing among tasks with similar visual or semantic characteristics. For example, as illustrated in Fig. 3, *Task 1* and *Task 2* (both involving opening drawer) are routed through the same gate but directed to different experts based on their specific operation requirements. In contrast, *Task 3*, which is semantically dissimilar, is routed through a different gate. This setup encourages the discovery of latent task clusters and provides the capacity to generalize to unseen tasks that share structural similarities with seen ones, thereby enhancing the transferability and robustness of TaskMoE. Notably, all tasks share a common pool of  $N_E$  experts, and for each input, only the top- $k$  experts (based on gating scores) are activated to guide task-specific visual feature extraction.

### 3.3. Multi-Viewpoint Exploration Policy

Our proposed **Multi-Viewpoint Exploration Policy (MVEP)** aims to select  $K$  viewpoints that maximally capture informative regions related to the manipulation target, thereby enhancing the accuracy of robotic action prediction. MVEPN takes as input the reconstructed point cloud  $\mathcal{P} \in \mathbb{R}^{N \times 3}$  and its associated RGB features  $\mathbf{F}_{\text{img}} \in \mathbb{R}^{N \times 3}$ , which are concatenated to form the input representation:

$$\mathbf{X} = \text{Concat}(\mathcal{P}, \mathbf{F}_{\text{img}}) \in \mathbb{R}^{N \times 6}, \quad (1)$$

where  $N$  denotes the number of 3D points. The fused representation  $\mathbf{X}$  is processed by a multi-layer perceptron (MLP), which predicts the parameters of  $K$  camera poses.

In this work, we represent each camera pose using a **look-at model** [54], which decouples the camera position and orientation via spherical coordinates. Therefore, the explored views are parameterized as 5-dimensional vectors  $\mathbf{p}^i = (\theta^i, \phi^i, r^i, \theta_{\text{up}}^i, \phi_{\text{up}}^i) \in \mathbb{R}^5$ , where  $(\theta, \phi, r)$  specify the camera center in spherical coordinates relative to the origin,  $(\theta_{\text{up}}, \phi_{\text{up}})$  define the orientation of the up vector, and  $i \in [0, K - 1]$  means the  $i_{\text{th}}$  view. So, all camera poses are  $\mathbf{p} = \{\mathbf{p}^i | i = 0, \dots, K - 1\}$ . Additionally, the camera is perpetually oriented toward the coordinate origin  $O(0, 0, 0)$ .

To facilitate gradient-based optimization of the viewpoint selection policy, we model each camera pose as a sample from a Gaussian distribution rather than predicting deterministic values. Specifically, for each of the  $K$  viewpoints, our MVEPN outputs the mean and log-standard deviation of a diagonal Gaussian distribution over the 5-dimensional camera pose parameters. Formally, the output for the  $i$ -th viewpoint is denoted as  $[\mu^i, \log \sigma^i]$ , where:

$$\begin{aligned} \mu^i &= [\mu_{\theta}^i, \mu_{\phi}^i, \mu_r^i, \mu_{\theta_{\text{up}}}^i, \mu_{\phi_{\text{up}}}^i], \\ \log \sigma^i &= [\log \sigma_{\theta}^i, \log \sigma_{\phi}^i, \log \sigma_r^i, \log \sigma_{\theta_{\text{up}}}^i, \log \sigma_{\phi_{\text{up}}}^i]. \end{aligned} \quad (2)$$

Then the explored camera pose  $\tilde{\mathbf{p}}^i = (\tilde{\theta}^i, \tilde{\phi}^i, \tilde{r}^i, \tilde{\theta}_{\text{up}}^i, \tilde{\phi}_{\text{up}}^i)$  is sampled using the reparameterization trick:

$$\tilde{\mathbf{p}}^i = \mu^i + \sigma^i \odot \epsilon^i, \quad \epsilon^i \sim \mathcal{N}(\mathbf{0}, \mathbf{I}), \quad (3)$$

which enables end-to-end training via backpropagation.

To ensure the sampled poses remain valid in the spherical coordinate system, we constrain each component to lie within a normalized range using the sigmoid function:

$$\begin{aligned} \tilde{\theta}^i &= \pi \cdot \sigma(\tilde{\theta}^i), & \tilde{\phi}^i &= 2\pi \cdot \sigma(\tilde{\phi}^i), \\ \tilde{r}^i &= r_{\min} + (r_{\max} - r_{\min}) \cdot \sigma(\tilde{r}^i), \\ \tilde{\theta}_{\text{up}}^i &= \pi \cdot \sigma(\tilde{\theta}_{\text{up}}^i), & \tilde{\phi}_{\text{up}}^i &= 2\pi \cdot \sigma(\tilde{\phi}_{\text{up}}^i), \end{aligned} \quad (4)$$

where  $\sigma(\cdot)$  denotes the sigmoid activation, and  $r_{\min}$  and  $r_{\max}$  define the allowable radial bounds.

### 3.4. Training Strategy

The entire training process of our Task-aware Virtual View Exploration (TVVE) model consists of three stages:

**Stage 1:** In the first stage, we train a fixed-view variant of TVVE using three default rendering perspectives: front, left, and top. This stage follows a similar training pipeline to RVT-2 [16], where the overall loss comprises several components. Specifically,  $\mathcal{L}_{hc}$  and  $\mathcal{L}_{hf}$  denote the cross-entropy losses over heatmaps produced by the coarse and fine grounding modules, respectively. The ground-truth heatmaps are generated using a truncated Gaussian distribution centered at the 2D projection of the ground-truth 3D location, as described in RVT [15]. Additionally, the loss includes the end-effector rotation loss  $\mathcal{L}_{rot}$ , computed as

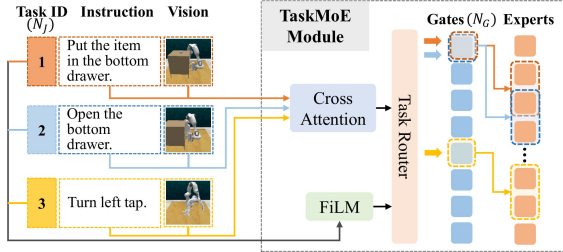


Figure 3. **Pipeline of the TaskMoE.** Our proposed TaskMoE takes *Task ID*, *Instruction*, and *Vision* as inputs to guide expert selection for task-specific visual representation learning. To improve scalability and generalization, we design a compact gating mechanism with  $N_G$  gates shared across  $N_J$  tasks ( $N_G < N_J$ ). This design allows tasks with similar action patterns (e.g., Task 1 and Task 2) to share the same gate, while assigning distinct gates to semantically diverse tasks (e.g., Task 3), thereby enabling effective feature specialization across a variety of manipulation tasks.

the cross-entropy loss for each of the Euler angles, as well as the gripper state loss  $\mathcal{L}_{gri}$  and collision indicator loss  $\mathcal{L}_{col}$ , both formulated as binary classification losses. The total objective for the first stage is given by:

$$\mathcal{L}_{s1} = \mathcal{L}_{hc} + \mathcal{L}_{hf} + \mathcal{L}_{rot} + \mathcal{L}_{gri} + \mathcal{L}_{col}. \quad (5)$$

**Stage 2:** In the second stage, we refine the Multi-View Exploration Policy (MVEP), using the fixed-view TVVE model trained in Stage 1 as a baseline. MVEP is optimized via the Proximal Policy Optimization (PPO) algorithm [42], which typically requires interaction with a physical environment to obtain reward feedback. To mitigate the high time cost, we introduce a novel *pseudo-environment interaction* mechanism. The details of the mechanism are presented in the supplementary materials.

Specifically, we treat the fixed-view TVVE as a reference model to supervise the training of MVEP. Given the same observations and instructions, the reference model yields losses  $\mathcal{L}_{ref} = [\mathcal{L}'_{hf}, \mathcal{L}'_{rot}, \mathcal{L}'_{gri}, \mathcal{L}'_{col}]$ . In contrast, MVEP generates dynamic viewpoints for action prediction, resulting in losses  $\mathcal{L}_{TVVE} = [\mathcal{L}'_{hf}, \mathcal{L}'_{rot}, \mathcal{L}'_{gri}, \mathcal{L}'_{col}]$ . Taking the reference model as a performance lower bound, our objective is to make  $\mathcal{L}_{TVVE}$  smaller than  $\mathcal{L}_{ref}$ . The first reward term is therefore defined as:

$$r_0 = \mathcal{L}_{ref} - \mathcal{L}_{TVVE}. \quad (6)$$

In addition to the task loss reward, we incorporate a confidence-based reward derived from the fine grounding module. Specifically, we compute the negative average entropy across the grounding heatmaps:

$$r_1 = -\frac{1}{K} \sum_{i=1}^K \mathcal{H}(\text{softmax}(\mathbf{H}_i)), \quad (7)$$

where  $\mathcal{H}$  denotes the entropy function and  $\mathbf{H}_i$  is the heatmap for view  $i$  from the fine grounding module.

To further encourage viewpoint diversity, we introduce an additional reward based on the average pairwise cosine distance between camera positions:

$$r_2 = \frac{1}{K(K-1)} \sum_{i \neq j} (1 - \cos(\mathbf{p}_i, \mathbf{p}_j)), \quad (8)$$

where  $\mathbf{p}_i$  represents the camera position for view  $i$ .

The overall reward is computed by adaptively normalizing and aggregating all components:

$$r = \sum_{i=0}^2 w_i \cdot \mathcal{N}(r_i), \quad (9)$$

where  $w_i$  are learnable component weights and  $\mathcal{N}$  is an online normalization operator. The adaptive normalization maintains the mean and variance of each component using the Welford algorithm [51] for normalization, and clips the reward to the range  $[-10, 10]$  to ensure training stability.

In this stage, only MVEP is trainable, and all the other components of TVVE are frozen.

**Stage 3:** To enable MVEP to better adapt to action generation, we further fine-tune the entire TVVE model, excluding MVEP, using the same loss functions as in Stage 1.

## 4. Experiments

To comprehensively assess the effectiveness and generalization of our Task-aware Virtual View Exploration(TVVE), we perform extensive experiments across both simulated and real-world environments.

### 4.1. Datasets and Experimental Setups

**Simulation.** Our experiments are conducted on **RLBench** dataset [22] and **RLBench-OG**.

**RLBench** is a multi-task learning benchmark implemented in the CoppeliaSim simulator featuring a 7-degree-of-freedom (7-DoF) Franka Emika Panda robot in a tabletop environment. Its observations consist of RGB-D images ( $128 \times 128$ ) captured from four fixed views, including frontal, left shoulder, right shoulder, and wrist-mounted. The action space represents the end-effector pose as  $\mathbf{a} = (\mathbf{p}_{xyz}, \mathbf{q}_{rot}, g_{gripper}, c_{collision}) \in \mathbb{R}^7 \times \{0, 1\}^2$ , where  $\mathbf{p}_{xyz} \in \mathbb{R}^3$  denotes Cartesian coordinates,  $\mathbf{q}_{rot} \in \mathbb{R}^4$  is the quaternion rotation,  $g_{gripper} \in \{0, 1\}$  controls gripper state, and  $c_{collision} \in \{0, 1\}$  indicates collision. Following previous works [16, 52], we evaluate our method under two standard configurations: (1) a *multi-view setup* consisting of 18 manipulation tasks (2–60 variations each) with all four camera views, and (2) a *single-view setup* including 10 tasks observed only from the front RGB-D camera. The specific tasks are provided in the supplementary materials.

**RLBench-OG** is derived from RLBench and used for validate the robustness of our TVVE under occluded sce-

Method	Avg. SR (%) $\uparrow$	Avg. Rank $\downarrow$	Close Jar	Drag Stick	Insert Peg	Meat off Grill	Open Drawer	Place Cups	Place Wine	Push Buttons
C2F-ARM-BC [23] (CVPR)	20.1	9.67	24.0	24.0	4.0	20.0	20.0	0.0	8.0	72.0
PerAct [45] (CoRL)	49.4	7.06	55.2 $\pm$ 4.7	89.6 $\pm$ 4.1	5.6 $\pm$ 4.1	70.4 $\pm$ 2.0	88.0 $\pm$ 5.7	2.4 $\pm$ 3.2	44.8 $\pm$ 7.8	92.8 $\pm$ 3.0
HiveFormer [17] (CoRL)	45.0	8.22	52.0	76.0	0.0	80.0	52.0	0.0	80.0	84.0
PolarNet [8] (CoRL)	46.0	7.06	36.0	92.0	4.0	<b>100.0</b>	84.0	0.0	40.0	96.0
RVT [15] (CoRL)	62.9	5.28	52.0 $\pm$ 2.5	99.2 $\pm$ 1.6	11.2 $\pm$ 3.0	88.0 $\pm$ 2.5	71.2 $\pm$ 6.9	4.0 $\pm$ 2.5	91.0 $\pm$ 5.2	<b>100.0<math>\pm</math>0.0</b>
Act3D [14] (CoRL)	63.2	5.56	96.8 $\pm$ 3.0	80.8 $\pm$ 6.4	24.0 $\pm$ 8.4	95.2 $\pm$ 1.6	78.4 $\pm$ 11.2	3.2 $\pm$ 3.0	59.2 $\pm$ 9.3	93.6 $\pm$ 2.0
3D Diffuser Actor [25] (CoRL)	81.3	3.0	96.0 $\pm$ 2.5	<b>100.0<math>\pm</math>0.0</b>	65.6 $\pm$ 4.1	96.8 $\pm$ 1.6	89.6 $\pm$ 4.1	24.0 $\pm$ 7.6	93.6 $\pm$ 4.8	98.4 $\pm$ 2.0
RVT2 [16] (RSS)	81.4	2.89	<b>100.0<math>\pm</math>0.0</b>	99.0 $\pm$ 1.7	40.0 $\pm$ 0.0	<b>99.0<math>\pm</math>1.0</b>	74.0 $\pm$ 11.8	38.0 $\pm$ 4.5	<b>95.0<math>\pm</math>3.3</b>	<b>100.0<math>\pm</math>0.0</b>
ARP [55] (RA-L)	81.6	2.83	97.6	88.0	53.2	96.0	<b>90.4</b>	48.0	92.0	<b>100.0</b>
<b>TVVE (Ours)</b>	<b>86.6</b>	<b>2.17</b>	<b>100.0<math>\pm</math>0.0</b>	<b>100.0<math>\pm</math>0.0</b>	<b>98.0<math>\pm</math>2.8</b>	94.0 $\pm$ 2.8	90.0 $\pm$ 2.8	<b>54.0<math>\pm</math>2.8</b>	92.0 $\pm$ 5.7	<b>100.0<math>\pm</math>0.0</b>

Method	Put in Cupboard	Put in Drawer	Put in Safe	Screw Bulb	Slide Block	Sort Shape	Stack Blocks	Stack Cups	Sweep to Dustpan	Turn Tap
C2F-ARM-BC [23] (CVPR)	0.0	4.0	12.0	8.0	16.0	8.0	0.0	0.0	0.0	68.0
PerAct [45] (CoRL)	28.0 $\pm$ 4.4	51.2 $\pm$ 4.7	84.0 $\pm$ 3.6	17.6 $\pm$ 2.0	74.0 $\pm$ 13.0	16.8 $\pm$ 4.7	26.4 $\pm$ 3.2	2.4 $\pm$ 2.0	52.0 $\pm$ 0.0	88.0 $\pm$ 4.4
HiveFormer [17] (CoRL)	32.0	68.0	76.0	8.0	64.0	12.0	4.0	0.0	28.0	80.0
PolarNet [8] (CoRL)	12.0	32.0	84.0	44.0	56.0	12.0	8.0	8.0	52.0	80.0
RVT [15] (CoRL)	49.6 $\pm$ 3.2	88.0 $\pm$ 5.7	91.2 $\pm$ 3.0	48.0 $\pm$ 5.7	81.6 $\pm$ 5.4	36.0 $\pm$ 2.5	28.8 $\pm$ 3.9	26.4 $\pm$ 8.2	72.0 $\pm$ 0.0	93.6 $\pm$ 4.1
Act3D [14] (CoRL)	67.2 $\pm$ 3.0	91.2 $\pm$ 6.9	95.2 $\pm$ 4.0	32.8 $\pm$ 6.9	96.0 $\pm$ 2.5	29.6 $\pm$ 3.2	4.0 $\pm$ 3.6	9.6 $\pm$ 6.0	86.4 $\pm$ 6.5	94.4 $\pm$ 2.0
3D Diffuser Actor [25] (CoRL)	<b>85.6<math>\pm</math>4.1</b>	96.0 $\pm$ 3.6	<b>97.6<math>\pm</math>2.0</b>	82.4 $\pm$ 2.0	97.6 $\pm$ 3.2	44.0 $\pm$ 4.4	68.3 $\pm$ 3.3	47.2 $\pm$ 8.5	84.0 $\pm$ 4.4	99.2 $\pm$ 1.6
RVT2 [16] (RSS)	66.0 $\pm$ 4.5	96.0 $\pm$ 0.0	96.0 $\pm$ 2.5	<b>88.0<math>\pm</math>4.9</b>	92.0 $\pm$ 2.8	35.0 $\pm$ 2.8	<b>80.0<math>\pm</math>2.8</b>	<b>69.0<math>\pm</math>5.9</b>	<b>100.0<math>\pm</math>0.0</b>	99.0 $\pm$ 1.7
ARP [55] (RA-L)	68.0	99.2	94.4	85.6	98.4	35.2	55.2	76.8	90.4	<b>100.0</b>
<b>TVVE (Ours)</b>	74.0 $\pm$ 8.5	<b>100.0<math>\pm</math>0.0</b>	78.0 $\pm$ 2.8	86.0 $\pm$ 2.8	<b>100.0<math>\pm</math>0.0</b>	<b>62.0<math>\pm</math>8.5</b>	74.0 $\pm$ 2.8	64.0 $\pm$ 5.7	92.0 $\pm$ 5.7	<b>100.0<math>\pm</math>0.0</b>

Table 1. **Performance comparison across 18 tasks in RLbench under the multi-view setup.** Our method achieves a substantial improvement in the average success rate. Moreover, the lower average rank of 2.17 demonstrates the superior overall performance and better generalization ability of TVVE across all 18 tasks.

	Avg. SR (%) $\uparrow$	Avg. Rank $\downarrow$	close jar	open drawer	sweep to dustpan	meat off grill	turn tap	slide block	put in drawer	drag stick	push buttons	stack blocks
GNFactor [52] (CoRL)	31.7	4.90	25.3	76.0	28.0	57.3	50.7	20.0	0.0	37.3	18.7	4.0
Act3D [14] (CoRL)	65.3	3.35	52.0 $\pm$ 5.7	84.0 $\pm$ 8.6	80.0 $\pm$ 9.8	66.7 $\pm$ 1.9	64.0 $\pm$ 5.7	<b>100.0<math>\pm</math>0.0</b>	54.7 $\pm$ 3.8	86.7 $\pm$ 1.9	64.0 $\pm$ 1.9	0.0 $\pm$ 0.0
3D Diffuser Actor [25] (CoRL)	78.4	2.20	82.7 $\pm$ 1.9	<b>89.3<math>\pm</math>7.5</b>	<b>94.7<math>\pm</math>1.9</b>	88.0 $\pm$ 5.7	80.0 $\pm$ 8.6	92.0 $\pm$ 0.0	77.3 $\pm$ 3.8	<b>98.7<math>\pm</math>1.9</b>	69.3 $\pm$ 5.0	12.0 $\pm$ 3.7
RVT2 [16] (RSS)	82.7 $\pm$ 0.7	2.40	96.0 $\pm$ 0.0	78.7 $\pm$ 3.8	73.3 $\pm$ 5.0	<b>93.3<math>\pm</math>1.9</b>	<b>93.3<math>\pm</math>3.8</b>	89.3 $\pm$ 1.9	73.3 $\pm$ 1.9	76.0 $\pm$ 0.0	<b>96.0<math>\pm</math>0.0</b>	<b>57.3<math>\pm</math>3.8</b>
<b>TVVE (Ours)</b>	<b>83.2<math>\pm</math>1.7</b>	<b>2.15</b>	<b>100.0<math>\pm</math>0.0</b>	84.0 $\pm$ 5.7	94.0 $\pm$ 2.8	92.0 $\pm$ 0.0	92.0 $\pm$ 5.7	90.0 $\pm$ 2.8	<b>98.0<math>\pm</math>2.8</b>	50.0 $\pm$ 2.8	82.0 $\pm$ 2.8	50.0 $\pm$ 8.5

Table 2. **Performance comparison across 10 tasks in RLbench under the single-view setup.** Our TVVE achieves a substantial improvement in the average success rate compared to previous methods.

narios and its generalization capability in complex environments. RLbench-OG consists of two distinct suites: the *Occlusion Suite* and the *Generalization Suite*. We created variants across 10 tasks for evaluation. In the Occlusion Suite, we designed two experimental configurations: 1) Models are both trained and tested directly under the occluded task configurations; 2) Models are trained in the original RLbench task settings and then evaluated in a zero-shot manner under occluded conditions. For the Generalization Suite, models are trained in the original RLbench environment and subsequently evaluated in a zero-shot manner across various generalization settings. Each task is configured with 50 episodes for training. The mean success rate, evaluated on 25 episodes per task, is reported as mean  $\pm$  standard deviation across three independent experimental runs. For simulating occlusion, we introduce occluders or rotate manipulated objects to create occlusions from a frontal viewpoint. For generalization, we introduce perturbations by: 1) altering scene lighting, 2) changing the color and texture of the tabletop, 3) modifying the color and texture of the background, 4) adding distractors, and 5) adjusting the pose of the observation camera. For further details on RLbench-OG, please refer to the supplementary material.

**Real World.** To evaluate the generalization of our TVVE across different robotic platforms, we conducted experi-

ments on both the *Franka Research 3* and the *Dobot Nova 2*. For the Franka Research 3, a single third-person camera (ORBEC Femto Bolt) was mounted directly in front of the arm. For the Dobot Nova 2, three Intel RealSense depth cameras were used: an overhead lateral camera (D435i), a front lateral camera (D455), and a wrist-mounted camera on the right arm (D405), as illustrated in the supplementary materials. We designed five distinct manipulation tasks: *Pick Grape*, *Stack Bowls*, *Push Buttons*, *Collect Fruits*, and *Put Item In Drawer*. Expert demonstrations were collected with 50 episodes per task for training. To improve efficiency, only key frames from the demonstrations were retained. Additional details of the real-world experiments are provided in the supplementary materials.

**Implementation Settings.** In our experiments, we set the number of camera viewpoints to  $K = 3$ , the number of gates in TaskMoE to  $N_G = 8$ , and the number of task experts to  $N_E = 16$ . For each task, the top-2 experts are selected. TVVE was trained on 4 NVIDIA RTX A800 GPUs. During testing, tasks were sequentially evaluated on a single NVIDIA RTX A800 GPU, and the average success rate was computed.

## 4.2. Comparison with State-of-the-art Methods

To comprehensively evaluate the effectiveness of our TVVE, we conduct comparisons with a broad range of

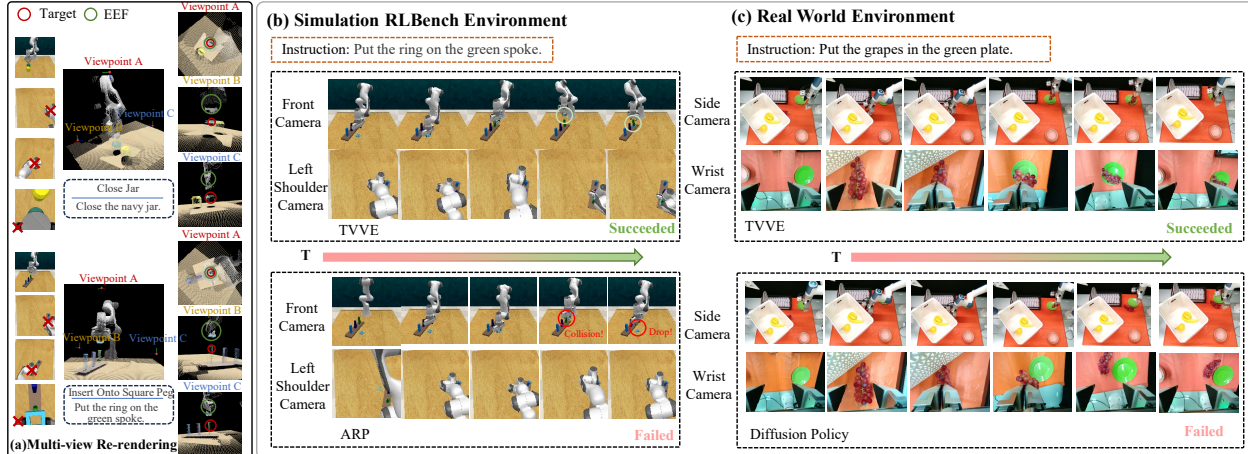


Figure 4. Visualization of our TVVE in the simulation RL Bench Environment and Diffusion Policy in the Real-world Environment. (a) In RL Bench, we visualize the re-rendering results of dynamic multi-view in the scenes for the *Close Jar* and *Insert Peg* tasks, where EEF in the figures denotes the end-effector. Visualizations of additional tasks are provided in the supplementary material. (b) Sample of *Insert Peg*. (c) Sample of *Pick Grape* in the real world.

Models	Avg. SR (%) $\uparrow$	Avg. Rank $\downarrow$	Occlusion 1	Occlusion 2	Light Color	Table Color	Table Texture	Distractor	Background Texture	Camera Pose
Diffusion Policy [9] (JRR)	23.8 $\pm$ 1.9	4.0	27.4 $\pm$ 0.8	23.4 $\pm$ 1.1	22.9 $\pm$ 0.8	22.5 $\pm$ 0.7	22.6 $\pm$ 0.5	24.4 $\pm$ 1.4	24.9 $\pm$ 1.2	22.2 $\pm$ 1.2
ARP [55] (RA-L)	63.7 $\pm$ 6.1	2.5	73.0 $\pm$ 1.6	52.6 $\pm$ 1.0	59.8 $\pm$ 0.8	62.7 $\pm$ 0.5	61.3 $\pm$ 1.0	62.4 $\pm$ 1.4	68.1 $\pm$ 1.6	69.7 $\pm$ 1.4
RVT2 [16] (RSS)	64.5 $\pm$ 8.3	2.1	72.8 $\pm$ 2.0	46.9 $\pm$ 0.4	60.8 $\pm$ 1.2	61.8 $\pm$ 1.1	64.0 $\pm$ 2.0	<b>63.4 <math>\pm</math> 0.2</b>	72.6 $\pm$ 0.6	<b>74.0 <math>\pm</math> 0.8</b>
<b>TVVE (Ours)</b>	<b>67.0 <math>\pm</math> 6.2</b>	<b>1.4</b>	<b>75.0 <math>\pm</math> 1.2</b>	<b>58.0 <math>\pm</math> 1.1</b>	<b>63.7 <math>\pm</math> 1.1</b>	<b>64.6 <math>\pm</math> 0.7</b>	<b>66.8 <math>\pm</math> 0.9</b>	60.2 $\pm$ 0.6	<b>74.3 <math>\pm</math> 0.9</b>	73.2 $\pm$ 0.9

Table 3. Comprehensive evaluation of model performance under occlusion and generalization settings in **RLBench-OG**, covering both zero-shot and trained scenarios. Detailed per-task success rates are provided in the supplementary material.

state-of-the-art approaches, including Diffusion Policy [9], C2F-ARM-BC [23], PerAct [45], Hiveformer [17], GNFactor [52], RVT [15], RVT2 [16], Act3D [14], 3D Diffuser Actor [25], and ARP [55]. We evaluate them both quantitatively and qualitatively across three benchmarks: RL Bench, RL Bench-OG, and real-world manipulation tasks.

**Comparisons on RL Bench.** Tables 1 and 2 present the quantitative results on RL Bench [22] under the multi-view and single-view setups, respectively. Our proposed TVVE consistently achieves significant improvements in average success rate across both settings. Specifically, TVVE attains an average success rate of **86.6%** under the multi-view setup, surpassing the previous state-of-the-art method ARP [55] by approximately **5%**. Notably, substantial gains are observed in tasks such as *Insert Peg* (from 65.6% to 98.0%) and *Sort Shape* (from 36.0% to 62.0%). A qualitative example of *Insert Peg* is illustrated in Fig. 4(a)(b). It shows that compared to ARP [55], which relies on fixed viewpoints, our TVVE dynamically renders more informative perspectives, effectively mitigating occlusions and collisions while providing richer context for more accurate action prediction, validating that dynamic “seeing” underpins robust “acting.” Moreover, as indicated by the lower average rank of **2.17** in Table 1, TVVE demonstrates superior overall performance across all 18 tasks, highlighting its enhanced generalization capability, which is primarily attributed to the proposed TaskMoE design.

Arm	Method	Avg. SR (%) $\uparrow$	Pick Grape	Stack Bowls	Push Buttons	Collect Fruits	Put Item In Drawer
Dobot	Diffusion Policy	68.0	90.0	70.0	70.0	50.0	60.0
	<b>TVVE (Ours)</b>	<b>88.0</b>	<b>100.0</b>	<b>90.0</b>	<b>100.0</b>	<b>70.0</b>	<b>80.0</b>
Franka	Diffusion Policy	58.0	90.0	50.0	60.0	40.0	50.0
	ARP	72.0	100.0	70.0	80.0	50.0	60.0
	<b>TVVE (Ours)</b>	<b>78.0</b>	<b>100.0</b>	<b>70.0</b>	<b>90.0</b>	<b>60.0</b>	<b>70.0</b>

Table 4. Comparison of task success rates for Dobot and Franka robots across different manipulation tasks. For more real-robot experiments, including robustness and generalization testing, please refer to the supplementary materials. \*Franka and Dobot adopt different experimental configurations.

**Comparisons on RL Bench-OG.** Table 3 highlights that TVVE achieves the best overall success rate (67.0%  $\pm$  6.2) and the best average rank (1.1) on RL Bench-OG, surpassing ARP (63.7%  $\pm$  6.1, rank 1.8) and the Diffusion Policy baseline (23.8%  $\pm$  1.9, rank 3.0). The advantage of our virtual-view exploration, dynamic virtual multi-view re-rendering and TaskMoE manifests consistently across perturbations: TVVE yields +2.0/+5.4 absolute gains over ARP for Occlusion 1/2, maintains higher resilience to background texture shifts (74.3%  $\pm$  0.9 vs. 68.1%  $\pm$  1.6), and preserves reliable execution under camera pose changes (73.2%  $\pm$  0.9 vs. 69.7%  $\pm$  1.4). These improvements confirm that learning task-aware viewpoints and decoupled visual representations mitigates the interference issues, leading to more robust manipulation under severe OOD disturbances.

**Comparisons on Real-World Tasks.** In Dobot robot experiment, compared to the baseline method Diffusion Policy (DP) [9], TVVE achieves superior performance across all tasks, attaining a significantly higher average success

Configuration	Avg. SR (%) $\uparrow$
TVVE (TaskMoE+MVEP)	<b>86.6</b>
w/o TaskMoE	85.6
Fixed Viewpoints	83.3
Random Viewpoints	8.9

Table 5. **Ablation study results on RL Bench multi-view setup.** Removing TaskMoE or replacing the explored viewpoints attained by MVEP with random or fixed ones degrades manipulation performance compared to the full TVVE with both components.

rate of 88.0% versus 68.0% for DP. Notable gains are observed in tasks such as “Push Buttons” (+30%) and “Stack Bowls” (+20%), underscoring the effectiveness of integrating task-aware visual planning into the policy framework. A qualitative example of *Pick Grape* is illustrated in Fig. 4(c). In Franka robot experiment, TVVE achieves the highest average success rate of 78.0%, outperforming both Diffusion Policy (58.0%) and ARP (72.0%). These results further demonstrate its strong adaptability in real-world scenarios. We report the success rates based on 10 trials for each task, with detailed results provided in Table 4. More real-world results are shown in the supplementary material.

#### 4.2.1. Ablation Studies.

In this section, we further analyze the impact of the TaskMoE, Multi-Viewpoint Exploration Policy (MVEP), and the hyperparameters  $K$  and  $r$ , supported by quantitative results in Tables 5, 6, and 7. Specifically, the results in Table 5 are obtained from experiments on all 18 RL Bench tasks, while those in Tables 6 and 7 are based on five representative tasks selected from RL Bench, namely *Put Item in Drawer*, *Turn Tap*, *Put Groceries in Cupboard*, *Put Money in Safe*, and *Close Jar*.

**Effectiveness of TaskMoE.** The TaskMoE module is designed to enhance multi-task generalization. From Table 5, removing TaskMoE from both the feature extraction and action generation components (*w/o TaskMoE*) leads to a moderate performance drop to 85.6%, underscoring its importance for multi-task representation learning. To further assess its generalization ability to OOD tasks unseen during training, additional results are presented in Table 6. The results show that TaskMoE not only improves performance on trained tasks but also facilitates transfer to unseen ones. Specifically, on tasks encountered during training, the model equipped with TaskMoE achieves an average success rate of 80.8%, outperforming the variant without TaskMoE (72.0%). This demonstrates its ability to learn and execute diverse, known tasks more effectively. For unseen tasks, the model without TaskMoE achieves a success rate of 60.0% on the new task *Open Drawer*, while the one with TaskMoE attains a higher success rate of 72.0%, highlighting its enhanced generalization capability.

**Effectiveness of MVEP.** The Multi-Viewpoint Exploration Policy (MVEP) is designed to dynamically explore better

TaskMoE	Avg. SR (%) $\uparrow$	Seen					Unseen Open drawer
		PID	TT	PGC	PMS	CJ	
$\checkmark$	80.8	100.0	100.0	32.0	88.0	84.0	72.0
$\times$	72.0	96.0	96.0	20.0	64.0	84.0	60.0

Table 6. **Experiments with and without TaskMoE.** TaskMoE not only improves performance on trained tasks but also enhances generalization to unseen tasks. Here, PID, TT, PGC, PMS, and CJ denote *Put Item in Drawer*, *Turn Tap*, *Put Groceries in Cupboard*, *Put Money in Safe*, and *Close Jar*, respectively.

$K$	$r$	PID	TT	PGC	PMS	CJ	Avg. SR (%) $\uparrow$
2	0.75~1.3	12.0	92.0	0.0	12.0	20.0	27.2
3	0.75~1.3	32.0	92.0	16.0	32.0	76.0	49.6
4	0.75~1.3	52.0	100.0	4.0	68.0	52.0	55.2
3	0.60~1.56	16.0	96.0	8.0	44.0	80.0	48.8
3	0.90~1.04	44.0	100.0	20.0	36.0	80.0	56.0

Table 7. Performance under different view numbers  $K$  and camera radial constraints  $r$ , which  $\Delta(r_{min}, r_{max}) = \pm 20\%$ . Task PID  $\rightarrow$  *Put item in drawer*, TT  $\rightarrow$  *Turn tap*, PGC  $\rightarrow$  *Put groceries in cupboard*, PMS  $\rightarrow$  *Put money in safe*, CJ  $\rightarrow$  *Close jar*.

camera viewpoints that reduce occlusion and provide more informative visual feature for improved robotic manipulation. To evaluate the effectiveness of MVEP, we replace the explored viewpoints with either fixed viewpoints used in RVT2 [16] or randomly selected ones. As shown in Table 5, the manipulation success rate drops from 86.6% to 83.3% when using fixed viewpoints, and further plummets to 8.9% when using random viewpoints. This significant degradation demonstrates that the learned viewpoint exploration policy in MVEP effectively identifies informative perspectives, which are crucial for accurate perception and robust action execution.

**Setting of  $K$  and  $r$ .** We conducted ablation studies on the camera radial constraint  $r$  and the number of views  $K$ . Compared to the baseline range (0.75 ~ 1.3)m, a tighter constraint (0.90 ~ 1.04)m improved performance, raising the average success rate from 49.6% to 56.0% (Table 7). A looser constraint (0.60 ~ 1.56)m slightly reduced performance (48.8%), indicating that a precise viewing distance range enhances task execution. Increasing the number of views from 2 to 4 under the baseline radial constraint consistently improved performance, with average success rates rising from 27.2% to 49.6% and 55.2%, respectively (Table 7). This demonstrates that multi-view observation mitigates occlusion and improves spatial perception. Considering computational cost, we chose  $K = 3$  as a balance.

## 5. Conclusion

Our TVVE framework establishes that dynamic view planning and task-aware representation learning significantly advance robotic manipulation capabilities. The MVEP’s viewpoint optimization effectively overcomes occlusion limitations in fixed-viewpoint systems, while TaskMoE’s specialized feature extraction mitigates multi-task interference. These contributions enhance performance across di-

verse manipulation challenges and enable meaningful generalization to novel tasks. However, the framework has some limitations: multi-view re-rendering slightly increases inference latency, and reliance on accurate global point clouds makes it challenging to handle reflective or transparent objects. Future work could integrate multi-sensor data and domain adaptation to improve real-world robustness.

## Acknowledgments

This work is supported by National Key Research and Development Program of China (2024YFE0203100), in part by the National Natural Science Foundation of China under Grant No.62572498 and No.62536010, in part by the open research fund of Pengcheng Laboratory under Grant 2025KF1B0050, in part by the Guangdong Basic and Applied Basic Research Foundation under Grant NO. 2025A1515011874. We also thank the National Supercomputer Center in Guangzhou for computational support.

## References

- [1] Kevin Black, Noah Brown, Danny Driess, Adnan Esmail, Michael Equi, Chelsea Finn, Niccolo Fusai, Lachy Groom, Karol Hausman, Brian Ichter, et al.  $\pi$ 0: A vision-language-action flow model for general robot control. *arXiv preprint ARXIV.2410.24164*, 2024. 1
- [2] Anthony Brohan, Noah Brown, Justice Carbajal, Yevgen Chebotar, Xi Chen, Krzysztof Choromanski, Tianli Ding, Danny Driess, Avinava Dubey, Chelsea Finn, et al. RT-2: Vision-language-action models transfer web knowledge to robotic control. *CoRL*, 2023. 1, 2
- [3] Anthony Brohan, Noah Brown, Justice Carbajal, Yevgen Chebotar, Joseph Dabis, Chelsea Finn, Keerthana Gopalakrishnan, Karol Hausman, Alexander Herzog, Jasmine Hsu, et al. RT-1: Robotics transformer for real-world control at scale. *Robotics: Science and Systems XIX*, 2023. 1
- [4] Qingwen Bu, Hongyang Li, Li Chen, Jisong Cai, Jia Zeng, Heming Cui, Maoqing Yao, and Yu Qiao. Towards synergistic, generalized, and efficient dual-system for robotic manipulation. *arXiv preprint arXiv:2410.08001*, 2024. 2
- [5] Qingwen Bu, Yanting Yang, Jisong Cai, Shenyan Gao, Guanghui Ren, Maoqing Yao, Ping Luo, and Hongyang Li. Univla: Learning to act anywhere with task-centric latent actions. *arXiv preprint arXiv:2505.06111*, 2025.
- [6] Jun Cen, Chaohui Yu, Hangjie Yuan, Yuming Jiang, Siteng Huang, Jiayan Guo, Xin Li, Yibing Song, Hao Luo, Fan Wang, et al. Worldvla: Towards autoregressive action world model. *arXiv preprint arXiv:2506.21539*, 2025.
- [7] Chi-Lam Cheang, Guangzeng Chen, Ya Jing, Tao Kong, Hang Li, Yifeng Li, Yuxiao Liu, Hongtao Wu, Jiafeng Xu, Yichu Yang, et al. Gr-2: A generative video-language-action model with web-scale knowledge for robot manipulation. *arXiv preprint arXiv:2410.06158*, 2024. 1, 2
- [8] Shizhe Chen, Ricardo Garcia, Cordelia Schmid, and Ivan Laptev. Polarnet: 3d point clouds for language-guided robotic manipulation. In *7th Conference on Robot Learning (CoRL 2023)*, 2023. 6, 16
- [9] Cheng Chi, Zhenjia Xu, Siyuan Feng, Eric Cousineau, Yilun Du, Benjamin Burchfiel, Russ Tedrake, and Shuran Song. Diffusion Policy: Visuomotor policy learning via action diffusion. *IJRR*, 2023. 1, 2, 7, 15
- [10] Murtaza Dalal, Min Liu, Walter Talbott, Chen Chen, Deepak Pathak, Jian Zhang, and Russ Salakhutdinov. Local policies enable zero-shot long-horizon manipulation. In *2nd CoRL Workshop on Learning Effective Abstractions for Planning*, 2024. 2
- [11] Marc Peter Deisenroth, Peter Englert, Jan Peters, and Dieter Fox. Multi-task policy search for robotics. In *2014 IEEE international conference on robotics and automation (ICRA)*, pages 3876–3881. IEEE, 2014. 2
- [12] Xinke Deng, Yu Xiang, Arsalan Mousavian, Clemens Eppner, Timothy Bretl, and Dieter Fox. Self-supervised 6d object pose estimation for robot manipulation. In *2020 IEEE International Conference on Robotics and Automation (ICRA)*, pages 3665–3671. IEEE, 2020. 2
- [13] Hao-Shu Fang, Chenxi Wang, Minghao Gou, and Cewu Lu. Graspnet-1billion: A large-scale benchmark for general object grasping. In *Proceedings of the IEEE/CVF conference on computer vision and pattern recognition*, pages 11444–11453, 2020. 2
- [14] Theophile Gervet, Zhou Xian, Nikolaos Gkanatsios, and Katerina Fragkiadaki. Act3d: 3d feature field transformers for multi-task robotic manipulation. In *Conference on Robot Learning*, pages 3949–3965. PMLR, 2023. 6, 7, 16
- [15] Ankit Goyal, Jie Xu, Yijie Guo, Valts Blukis, Yu-Wei Chao, and Dieter Fox. Rvt: Robotic view transformer for 3d object manipulation. *arXiv preprint arXiv:2306.14896*, 2023. 1, 4, 6, 7, 16
- [16] Ankit Goyal, Valts Blukis, Jie Xu, Yijie Guo, Yu-Wei Chao, and Dieter Fox. Rvt-2: Learning precise manipulation from few demonstrations. In *RSS 2024 Workshop: Data Generation for Robotics*, 2024. 1, 2, 3, 4, 5, 6, 7, 8, 15, 16
- [17] Pierre-Louis Guhur, Shizhe Chen, Ricardo Garcia Pinel, Makarand Tapaswi, Ivan Laptev, and Cordelia Schmid. Instruction-driven history-aware policies for robotic manipulations. In *Conference on Robot Learning*, pages 175–187. PMLR, 2023. 6, 7, 16
- [18] Yanjiang Guo, Jianke Zhang, Xiaoyu Chen, Xiang Ji, Yen-Jen Wang, Yucheng Hu, and Jianyu Chen. Improving vision-language-action model with online reinforcement learning. *arXiv preprint arXiv:2501.16664*, 2025. 3
- [19] Siddhant Haldar, Zhuoran Peng, and Lerrel Pinto. Baku: An efficient transformer for multi-task policy learning. *Advances in Neural Information Processing Systems*, 37: 141208–141239, 2024. 2
- [20] Zhi Hou, Tianyi Zhang, Yuwen Xiong, Hengjun Pu, Chengyang Zhao, Ronglei Tong, Yu Qiao, Jifeng Dai, and Yuntao Chen. Diffusion transformer policy. *arXiv preprint arXiv:2410.15959*, 2024. 1
- [21] Jiaheng Hu, Rose Hendrix, Ali Farhadi, Aniruddha Kembhavi, Roberto Martín-Martín, Peter Stone, Kuo-Hao Zeng, and Kiana Ehsani. Flare: Achieving masterful and adaptive

- robot policies with large-scale reinforcement learning fine-tuning. *arXiv preprint arXiv:2409.16578*, 2024. 3
- [22] Stephen James, Zicong Ma, David Rovick Arrojo, and Andrew J Davison. RL-Bench: The robot learning benchmark & learning environment. *IEEE Robotics and Automation Letters*, 2020. 2, 5, 7, 12
- [23] Stephen James, Kentaro Wada, Tristan Laidlow, and Andrew J Davison. Coarse-to-fine q-attention: Efficient learning for visual robotic manipulation via discretisation. In *Proceedings of the IEEE/CVF Conference on Computer Vision and Pattern Recognition*, pages 13739–13748, 2022. 6, 7, 16
- [24] Tsung-Wei Ke, Nikolaos Gkanatsios, and Katerina Fragkiadaki. 3d diffuser actor: Policy diffusion with 3d scene representations. *arXiv preprint arXiv:2402.10885*, 2024. 1
- [25] Tsung-Wei Ke, Nikolaos Gkanatsios, and Katerina Fragkiadaki. 3d diffuser actor: Policy diffusion with 3d scene representations. In *Conference on Robot Learning*, pages 1949–1974. PMLR, 2025. 6, 7, 16
- [26] Khimya Khetarpal, Matthew Riemer, Irina Rish, and Doina Precup. Towards continual reinforcement learning: A review and perspectives. *Journal of Artificial Intelligence Research*, 75:1401–1476, 2022. 3
- [27] Moo Jin Kim, Karl Pertsch, Siddharth Karamcheti, Ted Xiao, Ashwin Balakrishna, Suraj Nair, Rafael Rafailov, Ethan P Foster, Pannag R Sanketi, Quan Vuong, et al. OpenVLA: An open-source vision-language-action model. In *CoRL*, 2024. 1, 2
- [28] Peiyan Li, Yixiang Chen, Hongtao Wu, Xiao Ma, Xiangnan Wu, Yan Huang, Liang Wang, Tao Kong, and Tieniu Tan. BridgeVLA: Input-output alignment for efficient 3d manipulation learning with vision-language models. *arXiv preprint arXiv:2506.07961*, 2025.
- [29] Xinghang Li, Minghuan Liu, Hanbo Zhang, Cunjun Yu, Jie Xu, Hongtao Wu, Chilam Cheang, Ya Jing, Weinan Zhang, Huaping Liu, et al. Vision-language foundation models as effective robot imitators. *ICLR*, 2024. 2
- [30] Fanqi Lin, Ruiqian Nai, Yingdong Hu, Jiacheng You, Junming Zhao, and Yang Gao. Onetwovla: A unified vision-language-action model with adaptive reasoning. *arXiv preprint arXiv:2505.11917*, 2025.
- [31] Jiaming Liu, Hao Chen, Pengju An, Zhuoyang Liu, Renrui Zhang, Chenyang Gu, Xiaoqi Li, Ziyu Guo, Sixiang Chen, Mengzhen Liu, et al. Hybridvla: Collaborative diffusion and autoregression in a unified vision-language-action model. *arXiv preprint arXiv:2503.10631*, 2025. 1
- [32] Yang Liu, Weixing Chen, Yongjie Bai, Xiaodan Liang, Guanbin Li, Wen Gao, and Liang Lin. Aligning cyber space with physical world: A comprehensive survey on embodied ai. *IEEE/ASME Transactions on Mechatronics*, 2025. 1
- [33] Guanxing Lu, Wenkai Guo, Chubin Zhang, Yuheng Zhou, Haonan Jiang, Zifeng Gao, Yansong Tang, and Ziwei Wang. VLA-RL: Towards masterful and general robotic manipulation with scalable reinforcement learning. *arXiv preprint arXiv:2505.18719*, 2025. 3
- [34] Jianlan Luo, Zheyuan Hu, Charles Xu, You Liang Tan, Jacob Berg, Archit Sharma, Stefan Schaal, Chelsea Finn, Abhishek Gupta, and Sergey Levine. Serl: A software suite for sample-efficient robotic reinforcement learning. In *2024 IEEE International Conference on Robotics and Automation (ICRA)*, pages 16961–16969. IEEE, 2024. 3
- [35] Xiao Ma, Sumit Patidar, Iain Haughton, and Stephen James. Hierarchical diffusion policy for kinematics-aware multi-task robotic manipulation. In *Proceedings of the IEEE/CVF Conference on Computer Vision and Pattern Recognition*, pages 18081–18090, 2024. 2
- [36] Weixin Mao, Weiheng Zhong, Zhou Jiang, Dong Fang, Zhongyue Zhang, Zihan Lan, Haosheng Li, Fan Jia, Tiancai Wang, Haoqiang Fan, et al. Robomatrix: A skill-centric hierarchical framework for scalable robot task planning and execution in open-world. *arXiv preprint arXiv:2412.00171*, 2024. 2
- [37] Suraj Nair, Eric Mitchell, Kevin Chen, Silvio Savarese, Chelsea Finn, et al. Learning language-conditioned robot behavior from offline data and crowd-sourced annotation. In *CoRL*, 2022. 2
- [38] Ethan Perez, Florian Strub, Harm De Vries, Vincent Dumoulin, and Aaron Courville. Film: Visual reasoning with a general conditioning layer. In *AAAI*, 2018. 4
- [39] Evan Prianto, MyeongSeop Kim, Jae-Han Park, Ji-Hun Bae, and Jung-Su Kim. Path planning for multi-arm manipulators using deep reinforcement learning: Soft actor-critic with hindsight experience replay. *Sensors*, 20(20):5911, 2020. 2
- [40] Wilbert Pumacay, Ishika Singh, Jiafei Duan, Ranjay Krishna, Jesse Thomason, and Dieter Fox. The colosseum: A benchmark for evaluating generalization for robotic manipulation. In *RSS 2024 Workshop: Data Generation for Robotics*, 2024. 20
- [41] Aravind Rajeswaran, Vikash Kumar, Abhishek Gupta, Giulia Vezzani, John Schulman, Emanuel Todorov, and Sergey Levine. Learning complex dexterous manipulation with deep reinforcement learning and demonstrations. *arXiv preprint arXiv:1709.10087*, 2017. 3
- [42] John Schulman, Filip Wolski, Prafulla Dhariwal, Alec Radford, and Oleg Klimov. Proximal policy optimization algorithms. *arXiv preprint arXiv:1707.06347*, 2017. 5
- [43] Noam Shazeer, Azalia Mirhoseini, Krzysztof Maziarz, Andy Davis, Quoc Le, Geoffrey Hinton, and Jeff Dean. Outrageously large neural networks: The sparsely-gated mixture-of-experts layer. In *ICLR*, 2017. 2, 4, 14
- [44] Mohit Shridhar, Lucas Manuelli, and Dieter Fox. CLIPort: What and where pathways for robotic manipulation. In *CoRL*, 2022. 1, 2
- [45] Mohit Shridhar, Lucas Manuelli, and Dieter Fox. Perceiver-actor: A multi-task transformer for robotic manipulation. In *Conference on Robot Learning*, pages 785–799. PMLR, 2023. 1, 6, 7, 16
- [46] Chen Tang, Ben Abbatematteo, Jiaheng Hu, Rohan Chandra, Roberto Martín-Martín, and Peter Stone. Deep reinforcement learning for robotics: A survey of real-world successes. In *Proceedings of the AAAI Conference on Artificial Intelligence*, pages 28694–28698, 2025. 3
- [47] Octo Model Team, Dibya Ghosh, Homer Walke, Karl Pertsch, Kevin Black, Oier Mees, Sudeep Dasari, Joey Hejna, Tobias Kreiman, Charles Xu, et al. Octo: An open-

- source generalist robot policy. *Proceedings of Robotics: Science and Systems*, 2024. [1](#), [2](#)
- [48] Ikechukwu Uchendu, Ted Xiao, Yao Lu, Banghua Zhu, Mengyuan Yan, Joséphine Simon, Matthew Bennice, Chuyuan Fu, Cong Ma, Jiantao Jiao, et al. Jump-start reinforcement learning. In *International Conference on Machine Learning*, pages 34556–34583. PMLR, 2023. [3](#)
- [49] Lirui Wang, Jialiang Zhao, Yilun Du, Edward H Adelson, and Russ Tedrake. PoCo: Policy composition from and for heterogeneous robot learning. *CoRR*, 2024. [2](#)
- [50] Yixiao Wang, Yifei Zhang, Mingxiao Huo, Thomas Tian, Xiang Zhang, Yichen Xie, Chenfeng Xu, Pengliang Ji, Wei Zhan, Mingyu Ding, et al. Sparse diffusion policy: A sparse, reusable, and flexible policy for robot learning. In *Conference on Robot Learning*, pages 649–665. PMLR, 2025. [2](#), [4](#), [14](#)
- [51] Barry Payne Welford. Note on a method for calculating corrected sums of squares and products. *Technometrics*, 4(3): 419–420, 1962. [5](#)
- [52] Yanjie Ze, Ge Yan, Yueh-Hua Wu, Annabella Macaluso, Yuying Ge, Jianglong Ye, Nicklas Hansen, Li Erran Li, and Xiaolong Wang. Gnfactor: Multi-task real robot learning with generalizable neural feature fields. In *Conference on robot learning*, pages 284–301. PMLR, 2023. [2](#), [5](#), [6](#), [7](#), [16](#)
- [53] Yanjie Ze, Gu Zhang, Kangning Zhang, Chenyuan Hu, Muhan Wang, and Huazhe Xu. 3d diffusion policy: Generalizable visuomotor policy learning via simple 3d representations. In *ICRA*, 2024. [2](#)
- [54] A Zeng, P Florence, J Tompson, S Welker, J Chien, M At-tarian, T Armstrong, and I Krasin. Transporter networks: Rearranging the visual world for robotic manipulation. *RSS*, 2021. [4](#)
- [55] Xinyu Zhang, Yuhan Liu, Haonan Chang, Liam Schramm, and Abdeslam Boularias. Autoregressive action sequence learning for robotic manipulation. *IEEE Robotics and Automation Letters*, 2025. [2](#), [3](#), [6](#), [7](#), [16](#)
- [56] Bin Zhao, Yao Wu, Chengdong Wu, and Ruohuai Sun. Deep reinforcement learning trajectory planning for robotic manipulator based on simulation-efficient training. *Scientific Reports*, 15(1):8286, 2025. [2](#)
- [57] Tony Z Zhao, Vikash Kumar, Sergey Levine, and Chelsea Finn. Learning fine-grained bimanual manipulation with low-cost hardware. *RSS*, 2023. [1](#)

## Appendix

In this supplementary material, we provide additional details and results of our proposed TVVE to complement the main paper. The content is organized as follows:

- **Appendix A:** Real-world experimental details. Corresponding **demo videos** of the results are also included in the supplementary materials.
- **Appendix B:** Additional design details of TVVE, including TaskMoE, point cloud aggregation, camera pose parameterization, and the proposed pseudo-environment interaction mechanism.
- **Appendix C:** More simulation experimental details and results.
- **Appendix D:** Implementation details and information about the RL Bench [22] and RL Bench-OG. Additionally, we provide more visualized results, with corresponding **demo videos** included in the supplementary materials.
- **Appendix E:** Multi-view re-rendering visualization results.

### Appendix A. Real-World Experimental Details

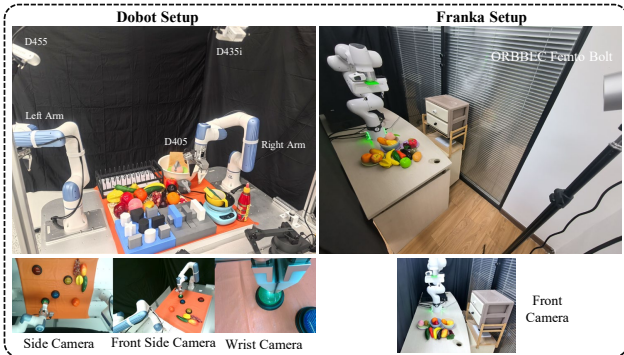


Figure 5. Real-World Environment Setup.

To validate the generalizability of the proposed TVVE in real-world deployment scenarios, we conducted experiments on two distinct robotic platforms: the Dobot Nova 2 and the Franka Research 3, employing differentiated camera configurations (multi-view and single-view) to comprehensively validate the scenarios. For the Dobot Nova 2, a multi-view setup consisting of three perspectives (side, front, and wrist-mounted) was used, whereas for the Franka robot, only a front view was utilized. Experimental results confirm that our TVVE can be successfully deployed on both platforms and outperforms both Diffusion Policy and ARP. Figure 5 illustrates the real-world deployment environments and the corresponding images from each viewpoint.

Across five real-world tasks—*Pick Grape*, *Stack Bowls*, *Push Buttons*, *Collect Fruits*, and *Put Item In Drawer*—our TVVE achieves strong performance. Notably, in the *pick-grape* task, it successfully executed the manipula-

tion even when the target was partially occluded in one viewpoint, demonstrating the advantage of our model in global perception capabilities. Corresponding demonstration videos are provided to facilitate a more intuitive understanding of the real-world outcomes.

Furthermore, to further evaluate the executive capability of our method across various types of tasks, we extended the experiments on the *Franka Research 3* platform to include ten additional tasks. These tasks encompass articulated object manipulation, deformable object manipulation, among others. Experimental results are summarized in Table 8, which indicate that our TVVE achieves high success rates, highlighting its adaptability and effectiveness across a diverse set of tasks.

### Real-World Robustness and Generalization Testing.

Arm	Method	Avg. SR (%) ↑	Seen	Inst.	Bkg.	Obj.	Occl.	Illum.
Dobot	Diffusion Policy	53.3	90.0	80.0	70.0	60.0	10.0	10.0
	TVVE (Ours)	<b>71.7</b>	100.0	100.0	90.0	90.0	20.0	30.0

Table 9. Performance comparison under different configurations on the Dobot robot. Abbreviations: Inst. (Unseen Instance), Bkg. (Unseen Background), Obj. (Unseen Object), Occl. (Heavy Occlusion), Illum. (Illumination Variation).

We conduct robustness testing on the real-world *Pick Grape* task on the *Dobot nova 2* robot, evaluating under various conditions including unseen instances, unseen backgrounds, unseen objects, heavy occlusion, and illumination variation. Throughout the experiments, heavy occlusion is identified as the primary cause of system failures. The results demonstrate that TVVE exhibits significantly better overall adaptability compared to the Diffusion Policy (DP) baseline. While both methods perform similarly in seen scenarios, TVVE substantially outperforms DP when confronted with unseen backgrounds, unseen objects, and especially under heavy occlusion. The success rates based on 10 trials for each configuration are reported, with quantitative comparisons detailed in Table 9.

### Details of Real-World Tasks.

We design real-world tasks to encompass as diverse operation types as possible, including grasping and placing, pressing/pushing, articulated object manipulation, rotation, deformable object manipulation, fine manipulation, tool usage, etc. The design details of each task are elaborated below.

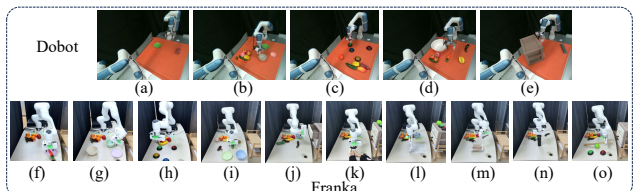


Figure 7. Real-World Tasks Setup.

Arm	Method	Avg. SR (%) ↑	Pick Place	Stack Bowls	Push Buttons	Collect Fruits	Put Item In Drawer	Rotate Handle	Fold Towel	Open Lip	Unscrew Bottle	Reach Drag
Franka	ARP	62.0%	10/10	7/10	8/10	5/10	6/10	3/10	5/10	7/10	3/10	8/10
	TVVE (Ours)	70.0%	10/10	7/10	9/10	6/10	7/10	3/10	5/10	9/10	5/10	9/10

Table 8. Task success rates for Franka robots across more manipulation tasks.



Figure 6. Visualization of Dobot and Franka Robots’ Execution Processes in Real-World Environments. In the figure, the T-axis represents the time axis, indicating the duration from the start to the end of the task. Each demonstration shows the following elements: side and wrist camera views for the Dobot robot, and a single front view for the Franka robot.

**Pick and Place.** On the table, there are fruits and a plate. The robot needs to pick up and place the specified fruits. Language instruction: Put the [FRUIT] into the [COLOR] plate. As shown in Fig. 7 (a)(f).

**Stack Bowls.** There are some bowls and a plate on the table. The robot needs to stack the bowls and plate in a specific order. Language instruction: Stack a [COLOR] bowl

and a [COLOR] bowl on a [COLOR] plate. As shown in Fig. 7 (b)(g).

**Push Buttons.** There are multiple buttons of different colors on the table. The robot needs to press the buttons in a specific sequence. Language instruction: Press the [COLOR] button, then the [COLOR] button, followed by the [COLOR] button, and finally the [COLOR] button. As

shown in Fig. 7 (c)(h).

**Collect Fruits.** There are various fruits on the table. The robot needs to collect the specified fruits into the specific target. Language instruction: Put a [FRUIT], a [FRUIT], and an [FRUIT] into the [COLOR] [TARGET]. As shown in Fig. 7 (d)(i).

**Put Item In Drawer.** There is a cabinet on the table. The robot needs to open the specified drawer, place the target object inside, and then close the drawer. Language instruction: Open the [Top/Middle/Bottom] drawer and put the [OBJECT] into it. As shown in Fig. 7 (e)(j).

**Rotate Handle.** The experimenter holds the handle, and the robot needs to rotate the handle by a certain angle. Language instruction: Rotate the handle clockwise. As shown in Fig. 7 (k).

**Fold Towel.** There is a towel on the table. The robot needs to pick up one corner of the towel and then fold it. Language instruction: Fold the towel. As shown in Fig. 7 (l).

**Open Lid.** There is a box on the table. The robot needs to pick up the lid and open it. Language instruction: Open the plastic lid of the biscuit case. As shown in Fig. 7 (m).

**Unscrew Bottle.** There is a bottle on the table. The robot needs to twist the cap to open the bottle. Language instruction: Unscrew the black bottle. As shown in Fig. 7 (n).

**Reach Drag.** There is a tool and an object to be manipulated on the table. The robot needs to use the tool to move the target object to the target position. Language instruction: Sweep the green apple into the gap between buttons using wood board. As shown in Fig. 7 (o).

## Appendix B. More design details of TVVE

### TaskMoE: Mathematical Principles and Operational Mechanism

To handle heterogeneous manipulation tasks, we introduce a task-aware Mixture-of-Experts (TaskMoE) that routes visual tokens through (i) a task-instruction-aware gate layer and (ii) a per-gate expert selector. Unlike prior MoE work [43, 50], TaskMoE decouples tasks from gates, decouples gates from experts, and adds semantic/entropy regularizers to avoid collapse.

**Cross-modal conditioning and FiLM.** Let  $\mathbf{V} \in \mathbb{R}^{S \times D}$  denote the sequence of visual tokens, where  $S$  is the number of spatial tokens and  $D$  is the feature dimension. Let  $\mathbf{I} \in \mathbb{R}^D$  be the language instruction embedding and  $\mathbf{t} \in \mathbb{R}^D$  the learnable embedding of the current task. We first fuse language into vision via cross-modal attention:

$$\mathbf{Q} = \mathbf{V}\mathbf{W}^Q, \quad \mathbf{K} = \mathbf{I}\mathbf{W}^K, \quad \mathbf{V}_a = \mathbf{I}\mathbf{W}^V, \quad (10)$$

$$\mathbf{V}' = \text{softmax}\left(\frac{\mathbf{Q}\mathbf{K}^\top}{\sqrt{d_k}}\right) \mathbf{V}_a, \quad (11)$$

where  $\mathbf{W}^Q, \mathbf{W}^K, \mathbf{W}^V \in \mathbb{R}^{D \times D}$  are projection matrices and  $d_k$  is the key dimension. The attention output  $\mathbf{V}' \in \mathbb{R}^{S \times D}$  is an instruction-attended visual feature. We then modulate channels with FiLM using globally pooled vision and the task embedding (here  $\text{GAP}(\cdot)$  is global average pooling over the  $S$  tokens):

$$\mathbf{c} = [\text{GAP}(\mathbf{V}'); \mathbf{t}] \in \mathbb{R}^{2D}, \quad (12)$$

$$\gamma, \beta = \text{MLP}(\mathbf{c}) \in \mathbb{R}^D \times \mathbb{R}^D, \quad (13)$$

$$\mathbf{V}_{\text{mod}} = \gamma \odot \mathbf{V} + \beta, \quad (14)$$

where  $\gamma$  and  $\beta$  are per-channel scaling and bias vectors and  $\odot$  denotes element-wise multiplication. The modulated feature  $\mathbf{V}_{\text{mod}} \in \mathbb{R}^{S \times D}$  serves as input to the gating network.

**Stage 1: Task-aware gates** ( $N_G \ll N_J$ ). We consider  $N_J$  tasks and  $N_G$  latent gates. Gates represent reusable skill clusters shared across tasks. A shared gate head scores  $N_G$  gates for each token and is modulated by a learnable task-gate assignment matrix  $\mathbf{A} \in \mathbb{R}^{N_J \times N_G}$ :

$$\mathbf{p}_g = \text{softmax}(\mathbf{V}_{\text{mod}} \mathbf{W}_g) \odot \text{softmax}(\mathbf{A}[j, :]), \quad (15)$$

where  $\mathbf{W}_g \in \mathbb{R}^{D \times N_G}$  is the gate projection and  $j \in \{1, \dots, N_J\}$  is the index of the current task. The matrix  $\mathbf{p}_g \in \mathbb{R}^{S \times N_G}$  contains, for each token, a probability distribution over gates. We select the top-1 gate per token (keeping top-2 for analysis) and apply a per-gate capacity constraint to prevent any gate from absorbing too many tokens.

**Stage 2: Per-gate expert selection** ( $N_E$  arbitrary). Given the chosen gate  $g \in \{1, \dots, N_G\}$ , we select experts from an independent pool of  $N_E$  experts. Each gate has its own expert head:

$$\mathbf{z}_e = \mathbf{V}_{\text{mod}} \mathbf{W}_{\text{exp}}[g] + \mathbf{b}_{\text{exp}}[g], \quad \mathbf{p}_e = \text{softmax}(\mathbf{z}_e), \quad (16)$$

where  $\mathbf{W}_{\text{exp}} \in \mathbb{R}^{D \times N_G \times N_E}$  and  $\mathbf{b}_{\text{exp}} \in \mathbb{R}^{N_G \times N_E}$  are the gate-expert projection and bias, and  $\mathbf{p}_e \in \mathbb{R}^{S \times N_E}$  gives, for each token, a probability distribution over experts under gate  $g$ . We keep top- $k$  experts per token (default  $k = 2$ ), optionally filter the second expert with a threshold/random policy, and enforce an expert capacity across the sequence. The resulting dispatch tensor aggregates these expert weights to route tokens to experts, and expert outputs are combined using the selected mixture weights.

**Regularization and loss.** Let  $\mathcal{L}_{\text{task}}$  denote the main imitation learning loss. We add balance, entropy, and semantic regularizers:

$$\mathcal{L} = \mathcal{L}_{\text{task}} + \lambda_g \mathcal{L}_{\text{bal-gate}} + \lambda_e \mathcal{L}_{\text{bal-exp}} \quad (17)$$

$$- \eta_g H(\mathbf{p}_g) - \eta_e H(\mathbf{p}_e) + \lambda_{\text{sem}} \mathcal{L}_{\text{sem}}(\mathbf{A}, \mathbf{I}), \quad (18)$$

where  $\mathcal{L}_{\text{bal-gate}}$  and  $\mathcal{L}_{\text{bal-exp}}$  penalize unbalanced gate/expert utilization,  $H(\mathbf{p}_g)$  and  $H(\mathbf{p}_e)$  are the entropies of the gate and expert distributions (encouraging diverse routing), and

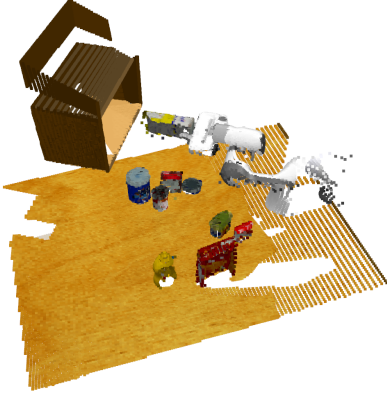


Figure 8. The aggregated full-scene point cloud of the *put\_groceries\_in\_cupboard* task from multiple viewpoints

$\mathcal{L}_{\text{sem}}(\mathbf{A}, \mathbf{I})$  aligns rows of the task–gate matrix  $\mathbf{A}$  with the similarity structure of instruction embeddings  $\mathbf{I}$  so that semantically related tasks share gates/experts. The scalars  $\lambda_g, \lambda_e, \eta_g, \eta_e, \lambda_{\text{sem}} \geq 0$  control the strength of each regularizer. Capacity clipping at both stages further prevents any single gate or expert from monopolizing the traffic.

**Scalability and specialization.** Because gates are decoupled from tasks and from experts, we can set the number of gates  $N_G$  and experts  $N_E$  independently (e.g.,  $N_G=8, N_E=16$ ). The gate layer captures coarse task affinity (each task uses only a few gates), while the expert layer refines routing inside each gate into task-specific specialists. Empirically, increasing  $N_E$  leads to finer skill factorization without leaving experts idle, validating the two-stage gate→expert design with entropy/semantic regularization.

### Point Cloud Aggregation.

In the RLbench dataset experiments, we select RGB-D images from four fixed viewpoints: *front*, *right\_shoulder*, *left\_shoulder*, and *wrist* as inputs. Following the approach of RVT-2 [16], we convert the depth maps from all viewpoints into point clouds in a global coordinate system using the intrinsic and extrinsic camera parameters. Subsequently, we perform multi-view point cloud aggregation and remove redundant points outside the workspace to obtain the final scene point cloud, as illustrated in Fig. 8.

### Pseudo-environment Interaction Mechanism.

To enable efficient policy optimization without physical environment interaction, we design a novel *pseudo-environment* interaction mechanism. As shown in Algorithm 1. The shadow network  $\pi_{\text{shadow}}$  (a frozen copy of the policy before training) processes observation  $\mathbf{o}$  to compute reference losses  $\mathcal{L}_{\text{ref}}$ . MVEP  $\pi_{\theta}$  processes  $\mathbf{o}$  to generate camera poses  $\mathbf{p}$  ( $\mathbf{p}$  as policy action), the rendered observation images from multi-view camera poses are fed into TaskMoE and TaskMoE-ARP (Autoregressive Action Policy) to compute the current policy losses  $\mathcal{L}_{\text{TVVE}}$ . The reward

---

### Algorithm 1 Pseudo-Environment Interaction

---

- 1: **Input:** Current observation  $\mathbf{o}$ , shadow network  $\pi_{\text{shadow}}$
  - 2: **Output:** Transition tuple  $\tau$
  - 3: # Compute reference loss
  - 4:  $\mathcal{L}_{\text{ref}} \leftarrow \pi_{\text{shadow}}(\mathbf{o})$
  - 5: # Generate camera poses & compute current model loss using TVVE
  - 6:  $\mathcal{L}_{\text{TVVE}}, \mathbf{p}, \log \pi_{\theta_{\text{old}}}(\mathbf{p}|\mathbf{o}), V_{\theta_{\text{old}}}(\mathbf{o}) \leftarrow \pi_{\theta_{\text{old}}}(\mathbf{o})$
  - 7: # Compute reward
  - 8:  $r \leftarrow \text{RewardCalculator}(\mathcal{L}_{\text{ref}}, \mathcal{L}_{\text{TVVE}}, \mathbf{p})$
  - 9: # Construct transition tuple
  - 10: **return**  $(\mathbf{o}, \mathbf{p}, r, \log \pi_{\theta_{\text{old}}}(\mathbf{p}|\mathbf{o}), V_{\theta_{\text{old}}}(\mathbf{o}))$
- 

$r$  is then calculated based on  $\mathcal{L}_{\text{ref}}, \mathcal{L}_{\text{TVVE}}$ , and  $\mathbf{p}$ . Finally, the experience tuple  $(\mathbf{o}, r, \mathbf{p}, \log \pi_{\theta_{\text{old}}}(\mathbf{p}|\mathbf{o}), V_{\theta_{\text{old}}}(\mathbf{o}))$  is stored in the replay buffer  $\mathcal{B}$  for policy updates. This approach enables batch environment interaction, leveraging existing demonstration data to improve policies and enhance data utilization efficiency.

### Camera Pose Parameterization.

The camera pose is mathematically represented using a **look-at model** defined by a 5-dimensional parameter vector  $\mathbf{p}^i = (\theta^i, \phi^i, r^i, \theta_{\text{up}}^i, \phi_{\text{up}}^i) \in \mathbb{R}^5 (i \in [0, K-1], K$  is number of camera viewpoint). This representation decouples camera position from orientation through spherical coordinates:

$$\mathbf{t}^i = \begin{bmatrix} x^i \\ y^i \\ z^i \end{bmatrix} = \begin{bmatrix} r^i \sin \theta^i \cos \phi^i \\ r^i \sin \theta^i \sin \phi^i \\ r^i \cos \theta^i \end{bmatrix} \quad (19)$$

where  $\mathbf{t}^i$  denotes the camera center position. The viewing direction is intrinsically defined as  $\mathbf{v}_{\text{look}}^i = -\mathbf{t}^i / \|\mathbf{t}^i\|_2$  toward the **origin**. The up-vector orientation is parameterized as:

$$\mathbf{v}_{\text{up}}^i = \begin{bmatrix} \sin \theta_{\text{up}}^i \cos \phi_{\text{up}}^i \\ \sin \theta_{\text{up}}^i \sin \phi_{\text{up}}^i \\ \cos \theta_{\text{up}}^i \end{bmatrix} \quad (20)$$

The final camera matrix is constructed via Gram-Schmidt orthogonalization between  $\mathbf{v}_{\text{look}}^i$  and  $\mathbf{v}_{\text{up}}^i$ .

## Appendix C. More Experimental Details and Results

### Baseline Details.

We compare with eleven state-of-the-art baselines on RL-Bench, RLbench-OG and Real-world, including both 2D and 3D approaches. For 2D methods, we include **Diffusion Policy** [9], which formulates robot policies as conditional

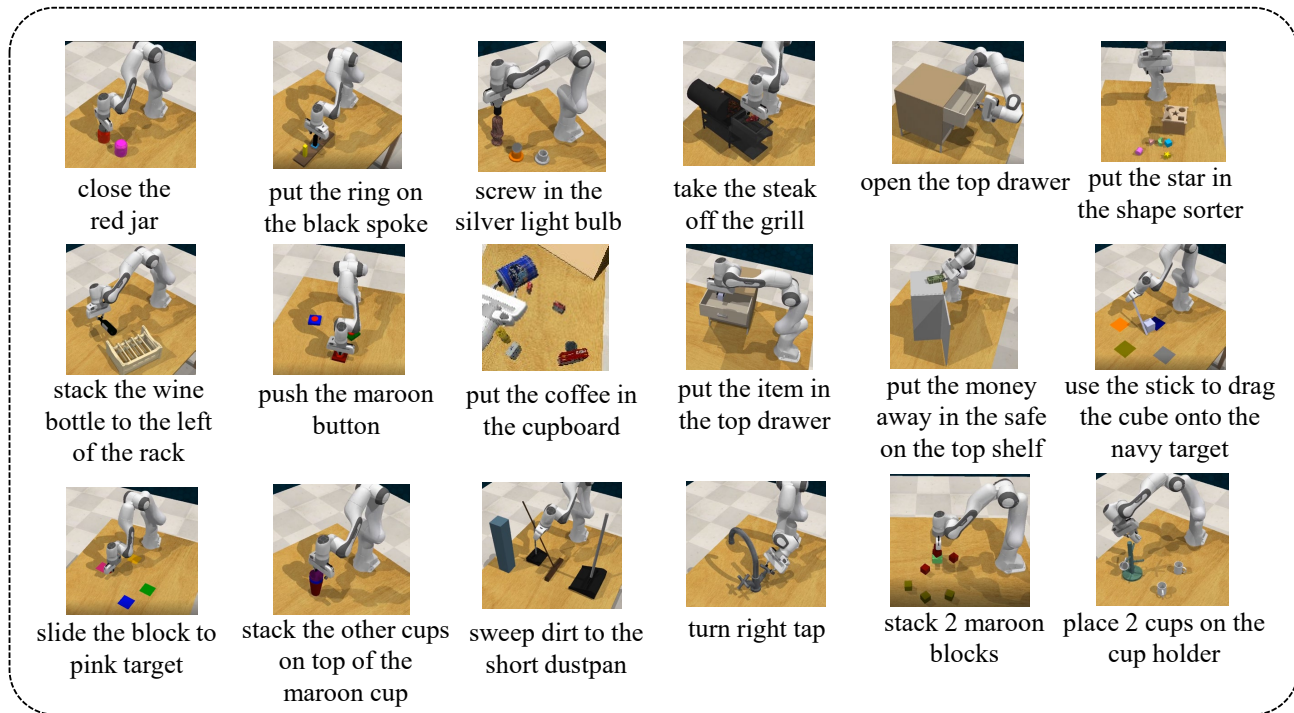


Figure 9. Demonstrations of 18 RL Bench tasks and their corresponding language instructions.

denoising diffusion processes. The 3D baselines comprise voxel-based methods: **C2F-ARM-BC** [23], which predicts actions in a coarse-to-fine manner via Q-value estimation; **PerAct** [45], which detects actions through global self-attention; **Hiveformer** [17], which employs attention across historical features; and **GNFactor** [52], which co-optimizes a neural scene representation with a PerAct-based policy. We also consider point-based methods: **PolarNet** [8], which computes dense point representations, and multi-view approaches: **RVT** [15], which fuses multi-view predictions via 3D back-projection, and its successor **RVT2** [16], which enhances precision and efficiency. Furthermore, we include **Act3D** [14], which uses coarse-to-fine 3D featurization (retrained by us for a fair comparison), **3D Diffuser Actor** [25], a 3D diffusion-based policy, and **ARP** [55], an autoregressive policy generating hybrid action sequences via a Chunking Causal Transformer.

### Implementation Details.

In the RL Bench *Multi-view setup* experiments, during the supervised pre-training phase, our experimental hyperparameter settings comply with APR[55]. In the offline reinforcement learning phase for MVEP, our hyperparameter configurations are detailed in Table 10.

### Performance-Efficiency Trade-off Analysis.

During inference, TVVE must predict dynamic multi-view camera poses and continuously adjust the rendering camera pose, resulting in a non-negligible computational overhead. To assess the practicality of the proposed TVVE model,

Hyperparameter	Value
<i>MVEP</i>	
$K$ number of the camera viewpoints	3
$N_{MVEP}$ The number of input point clouds for MVEP	2048
MVEP embedding size	512
<i>Train &amp; Eval</i>	
observation(RGBD)	$4 \times 128 \times 128 \times 4$
re-render image resolution	$224 \times 224$
maximum evaluation steps	25
train epochs	20
eval frequency	100
batch size	96
learning rate	$2.0e-6$
learning rate scheduler	cosine
optimizer	LAMB

Table 10. Hyperparameters for offline reinforcement learning training in RL Bench experiments.

Method	Average Success Rate (%)	Average Inference Time(s)
ARP	81.6	0.394
TVVE	86.6	0.436

Table 11. Comparison of the average success rate and inference time between ARP and TVVE across 18 tasks.

we compare its average task success rate and inference latency with those of the baseline model, ARP. The results, summarized in Table 11 on the RL Bench, show that TVVE

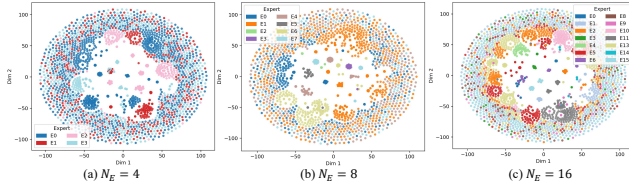


Figure 10. t-SNE visualization of instruction embeddings routed through the 4-expert (a), 8-expert (b) and 16-expert (c) TaskMoE. In the 4-expert TaskMoE (a), each expert bears a high workload, their specialization is limited, and it is difficult to achieve fine-grained partitioning. In the 8-expert TaskMoE (b), inner-region experts (E0, E1, E2, E3, E4, E5, E6, E7) form compact, semantically coherent clusters, while outer-ring embeddings are dominated by E1, E4 and E7, indicating fallback routing for diverse or weakly structured instructions. Compared to the 8-expert configuration, the 16-expert TaskMoE exhibits more balanced expert utilization.  $N_E$  denotes the number of experts.

achieves a higher average success rate than ARP, while the increase in inference latency remains relatively modest (approximately 10.7%). These findings suggest that TVVE effectively balances task performance and operational efficiency, with design elements such as sampling acceleration and camera caching playing a key role in enhancing model efficiency.

### Data Efficiency Analysis.

Method	20	40	80	100
ARP	$6.7 \pm 2.3$	$14.7 \pm 2.3$	$28.0 \pm 4.0$	$45.3 \pm 6.1$
TVVE (Ours)	<b><math>10.7 \pm 2.3</math></b>	<b><math>17.3 \pm 2.3</math></b>	<b><math>30.7 \pm 6.1</math></b>	<b><math>52.0 \pm 4.0</math></b>

Table 12. Success rate (mean  $\pm$  std %) comparison under varying numbers of demonstrations on the RLbench *Put in Cupboard* task.

We conduct a demonstration ablation study on the RLbench *Put in Cupboard* task. As shown in Table 12, TVVE consistently outperforms the baseline ARP across all demonstration sizes (20, 40, 80, and 100). Notably, the performance gap widens as the number of demonstrations increases, with TVVE achieving a success rate of  $52.0 \pm 4.0\%$  compared to  $45.3 \pm 6.1\%$  for ARP at 100 demonstrations. This trend demonstrates that while more data benefits both methods, the superior sample efficiency and final performance of TVVE are inherently due to our proposed architectural improvements, not simply the result of scaling the dataset.

### Results on RLbench-OG.

We conducted an evaluation of TVVE, RVT2, ARP, and Diffusion Policy on the RLbench-OG benchmark. Detailed performance across 10 tasks under 8 variations is presented in Tables 13, 14, 15, and 16. The reported success rates correspond to the mean  $\pm$  standard deviation from three independent trials.

### Experimental Results and Analysis on TaskMoE.

In the RLbench *Multi-view setup* experiments, we conducted individual ablation studies on the components of

TaskMoE, and visualized and analyzed the routing behavior of the gate-expert at both the **instruction-level** and **task-level**.

**Instruction-level Routing Behavior Analysis.** We compare the routing behavior of the 16-expert Task-MoE with the 4-expert and 8-expert configuration using instruction-level t-SNE embeddings, as shown in Fig. 10. The 16-expert model exhibits markedly improved semantic disentanglement: the embedding manifold contains a substantially larger number of compact and well-separated clusters, each corresponding to an expert with strong specialization. Expert utilization becomes significantly more balanced, with reduced reliance on fallback experts for long-tail or weakly structured instructions. The outer-ring region—typically occupied by generic or ambiguous instructions—is shared by a diverse subset of experts rather than collapsing onto one or two dominant experts. This indicates that the expanded expert capacity enables finer-grained semantic partitioning and mitigates routing collapse. In contrast, the 8-expert model shows partially collapsed routing behavior. Although several inner-region experts still form coherent semantic clusters, the outer ring is dominated by E1, E4 and E7, which assume the role of catch-all experts. Their dispersed and high-density presence suggests that the gate struggles to allocate long-tail and noisy instructions across multiple experts. Consequently, the semantic boundaries between experts remain coarse, limiting the degree of modularization and reducing the benefits of MoE specialization. Overall, the comparison demonstrates that increasing the number of experts from 8 to 16 leads to more stable routing, finer semantic granularity, and healthier expert balancing, thereby enabling a more expressive and disentangled mixture-of-experts structure.

**Task-level Routing Behavior Analysis.** We analyze the gate and expert routing behavior by visualizing the task-wise distributions. Such visualization allows us to examine whether different RLbench tasks activate distinct subsets of gates and experts, revealing the degree of task specialization, routing stability, and expert utilization diversity within the TaskMoE architecture.

Fig. 11 shows per-task top-1 gate/expert usage for  $N_E = 8$  (a,b) and  $N_E = 16$  (c,d). With 8 experts, every task settles on 1–2 gates (e.g., *place\_shape\_in\_shape\_sorter* and *put\_groceries\_in\_cupboard* both enter G3; *place\_cups* enters G2/G3), and all gates/experts are exercised, confirming the task-aware gate design learns a stable task  $\rightarrow$  gate partition without idle capacity. Increasing to 16 experts keeps the gate partition similar but further splits the downstream experts: tasks that shared a single expert at  $N_E = 8$  now route to distinct experts (e.g., *meat\_off\_grill* disperses over E1/E7 (from E1), *place\_shape\_in\_shape\_sorter* shifts to E8/E10

Task Name	Occlusion 1	Occlusion 2	Light Color	Table Color	Table Texture	Distractor	Background Texture	Camera Pose	Variant Mean
basketball_in_hoop	100.0 ± 0.0	100.0 ± 0.0	100.0 ± 0.0	92.0 ± 0.0	96.0 ± 0.0	70.0 ± 2.0	100.0 ± 0.0	100.0 ± 0.0	94.8 ± 9.8
scoop_with_spatula	88.0 ± 8.0	88.0 ± 5.7	64.0 ± 0.0	76.0 ± 0.0	86.0 ± 2.0	68.0 ± 4.0	92.0 ± 4.0	89.3 ± 3.8	81.4 ± 10.8
take_plate_off_colored_dish_rack	100.0 ± 0.0	98.7 ± 1.9	76.0 ± 4.0	94.0 ± 6.0	92.0 ± 0.0	100.0 ± 0.0	98.7 ± 1.9	100.0 ± 0.0	94.9 ± 8.2
water_plants	88.0 ± 4.0	26.7 ± 3.8	16.0 ± 4.0	16.0 ± 0.0	20.0 ± 4.0	22.7 ± 1.9	24.0 ± 4.0	24.0 ± 3.3	29.7 ± 22.6
block_pyramid	8.0 ± 8.0	0.0 ± 0.0	22.0 ± 6.0	8.0 ± 0.0	8.0 ± 0.0	12.0 ± 0.0	16.0 ± 4.0	18.0 ± 6.0	11.5 ± 7.9
solve_puzzle	2.0 ± 2.0	0.0 ± 0.0	14.0 ± 6.0	14.0 ± 2.0	10.0 ± 2.0	12.0 ± 0.0	24.0 ± 0.0	22.0 ± 2.0	12.2 ± 8.3
take_usb_out_of_computer	100.0 ± 0.0	100.0 ± 0.0	97.3 ± 1.9	100.0 ± 0.0	96.0 ± 0.0	82.7 ± 1.9	100.0 ± 0.0	100.0 ± 0.0	97.0 ± 5.7
close_drawer	100.0 ± 0.0	100.0 ± 0.0	92.0 ± 0.0	96.0 ± 0.0	96.0 ± 0.0	98.7 ± 1.9	98.7 ± 1.9	98.7 ± 1.9	97.5 ± 2.8
straighten_ropes	64.0 ± 0.0	0.0 ± 0.0	58.0 ± 2.0	50.0 ± 2.0	64.0 ± 8.0	36.0 ± 0.0	89.3 ± 5.0	80.0 ± 4.0	55.2 ± 26.2
toilet_seat_down	100.0 ± 0.0	66.7 ± 8.2	97.3 ± 1.9	100.0 ± 0.0	100.0 ± 0.0	100.0 ± 0.0	100.0 ± 0.0	100.0 ± 0.0	95.5 ± 11.3

Task Mean: 75.0 ± 1.2, 58.0 ± 1.1, 63.7 ± 1.1, 64.6 ± 0.7, 66.8 ± 0.9, 60.2 ± 0.6, 74.3 ± 0.9, 73.2 ± 0.9, 67.0 ± 6.2

Table 13. Success Rates of TVVE under Different Perturbations of RL-Bench-OG.

Task Name	Occlusion 1	Occlusion 2	Light Color	Table Color	Table Texture	Distractor	Background Texture	Camera Pose	Variant Mean
basketball_in_hoop	100.0 ± 0.0	100.0 ± 0.0	88.8 ± 1.6	96.0 ± 0.0	99.2 ± 1.6	88.0 ± 0.0	100.0 ± 0.0	100.0 ± 0.0	96.5 ± 4.8
scoop_with_spatula	82.7 ± 7.5	84.0 ± 6.5	75.4 ± 2.6	84.0 ± 5.7	88.0 ± 5.7	76.0 ± 4.0	98.0 ± 2.0	96.0 ± 0.0	85.5 ± 7.7
take_plate_off_colored_dish_rack	98.7 ± 1.9	65.3 ± 6.8	60.0 ± 4.6	88.8 ± 3.9	84.8 ± 4.7	100.0 ± 0.0	100.0 ± 0.0	100.0 ± 0.0	87.2 ± 15.2
water_plants	72.0 ± 8.6	20.0 ± 5.7	12.0 ± 5.1	9.6 ± 9.3	23.0 ± 5.9	22.0 ± 2.0	26.0 ± 2.0	32.0 ± 0.0	27.1 ± 18.3
block_pyramid	4.0 ± 3.3	0.0 ± 0.0	0.0 ± 0.0	0.0 ± 0.0	0.0 ± 0.0	0.0 ± 0.0	0.0 ± 0.0	0.0 ± 0.0	0.5 ± 1.3
solve_puzzle	0.0 ± 0.0	0.0 ± 0.0	9.3 ± 3.0	8.0 ± 3.6	12.0 ± 5.1	20.0 ± 0.0	16.0 ± 3.3	25.3 ± 3.8	11.3 ± 8.4
take_usb_out_of_computer	100.0 ± 0.0	100.0 ± 0.0	100.0 ± 0.0	100.0 ± 0.0	95.2 ± 1.6	98.0 ± 2.0	98.7 ± 1.9	100.0 ± 0.0	99.0 ± 1.6
close_drawer	100.0 ± 0.0	100.0 ± 0.0	99.3 ± 1.5	97.6 ± 2.0	98.4 ± 2.0	96.0 ± 0.0	100.0 ± 0.0	100.0 ± 0.0	98.9 ± 1.4
straighten_ropes	70.7 ± 10.0	0.0 ± 0.0	56.7 ± 5.8	37.6 ± 5.4	44.0 ± 5.1	36.0 ± 0.0	86.7 ± 5.0	88.0 ± 4.0	52.5 ± 27.6
toilet_seat_down	100.0 ± 0.0	0.0 ± 0.0	100.0 ± 0.0	100.0 ± 0.0	100.0 ± 0.0	98.0 ± 2.0	100.0 ± 0.0	100.0 ± 0.0	87.2 ± 33.0

Task Mean: 72.8 ± 2.0, 46.9 ± 0.4, 60.8 ± 1.2, 61.8 ± 1.1, 64.0 ± 2.0, 63.4 ± 0.2, 72.6 ± 0.6, 74.0 ± 0.8, 64.5 ± 8.3

Table 14. Success Rates of RVT2 under Different Perturbations of RL-Bench-OG.

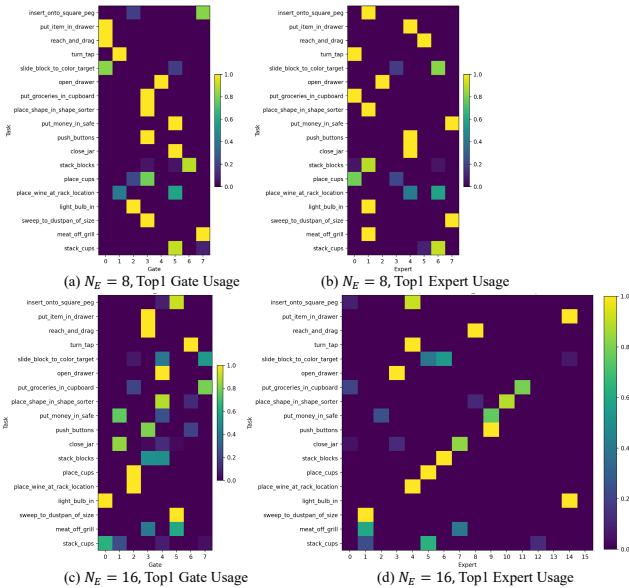


Figure 11. Task-wise gate and expert usage visualization for the proposed MoE layer. Both 8-expert (a,b) and 16-expert (c,d) configurations demonstrate clear task-dependent routing, while larger expert capacity allows finer-grained specialization without leading to expert collapse.

(from E1), *put\_money\_in\_safe* to E2/E9 (from E7), yielding finer skill specialization. This validates that the two-stage gate→expert routing, combined with entropy/semantic regularization and a larger  $N_E$ , not only provides additional capacity that is fully utilized without collapsing to a few experts but also enhances sparsity, which optimizes computational efficiency and improves generalization by distribut-

ing representations more distinctly.

Moreover, Fig. 11(c,d) shows the two-stage router differentiates fine-grained skills even when tasks share the same gate. For example, the semantically related tasks *place\_cups* and *place\_wine\_at\_rack\_location* both enter the same gate (G2) at  $N_E = 16$ , yet their traffic is split to different experts downstream (e.g., *place\_cups* to E5 vs. *place\_wine\_at\_rack\_location* to E4). This demonstrates that the gate layer captures coarse task affinity while the expert layer refines the routing to task-specific specialists, confirming the effectiveness of the two-stage gate→expert design in achieving fine-grained routing without losing shared structure.

**Generalization.** We conduct experiments in RL-Bench, training on tasks such as *Insert\_Peg* and *Put\_Item\_Drawer*, and others, and is subsequently evaluated on a set of unseen tasks. Our model achieves high success rates in completing certain tasks not encountered during training, demonstrating the generalization capability of our architecture. The results are shown in Table 17.

## Appendix D. Implementation details and information about the RL-Bench and RL-Bench-OG RL-Bench.

To evaluate the effectiveness and generalization capability of the proposed TVVE for multi-task robotic manipulation, we conduct experiments on 18 diverse tasks from the RL-Bench benchmark, including *close\_jar*, *stack\_blocks*, and

Task Name	Occlusion 1	Occlusion 2	Light Color	Table Color	Table Texture	Distractor	Background Texture	Camera Pose	Variant Mean
basketball_in_hoop	100.0 ± 0.0	100.0 ± 0.0	86.0 ± 2.0	76.0 ± 0.0	86.0 ± 2.0	84.0 ± 0.0	100.0 ± 0.0	100.0 ± 0.0	91.5 ± 9.0
scoop_with_spatula	88.0 ± 4.0	76.0 ± 8.0	62.0 ± 2.0	78.0 ± 2.0	86.0 ± 2.0	82.0 ± 2.0	86.7 ± 10.0	84.0 ± 8.0	80.3 ± 9.8
take_plate_off_colored_dish_rack	100.0 ± 0.0	76.0 ± 4.0	74.0 ± 6.0	96.0 ± 0.0	94.0 ± 6.0	100.0 ± 0.0	100.0 ± 0.0	100.0 ± 0.0	92.5 ± 10.9
water_plants	66.0 ± 14.0	10.0 ± 2.0	10.0 ± 2.0	12.0 ± 0.0	10.7 ± 3.8	13.3 ± 7.5	16.0 ± 8.0	21.3 ± 3.8	19.9 ± 19.0
block_pyramid	14.0 ± 2.0	0.0 ± 0.0	1.0 ± 1.7	5.3 ± 3.8	0.8 ± 1.6	2.4 ± 3.2	2.0 ± 3.5	6.4 ± 8.2	4.0 ± 5.7
solve_puzzle	0.0 ± 0.0	0.0 ± 0.0	14.0 ± 2.0	8.0 ± 0.0	6.0 ± 2.0	16.0 ± 8.6	8.0 ± 4.0	14.0 ± 6.0	8.2 ± 7.1
take_usb_out_of_computer	100.0 ± 0.0	100.0 ± 0.0	100.0 ± 0.0	98.0 ± 2.0	96.0 ± 0.0	94.0 ± 2.0	100.0 ± 0.0	98.7 ± 1.9	98.3 ± 2.4
close_drawer	100.0 ± 0.0	100.0 ± 0.0	96.0 ± 0.0	98.0 ± 2.0	100.0 ± 0.0	94.0 ± 2.0	100.0 ± 0.0	100.0 ± 0.0	98.5 ± 2.4
straighten_ropes	62.0 ± 6.0	4.0 ± 0.0	60.0 ± 0.0	60.0 ± 0.0	46.0 ± 6.0	42.0 ± 6.0	68.0 ± 8.0	74.0 ± 2.0	52.0 ± 21.2
toilet_seat_down	100.0 ± 0.0	60.0 ± 4.0	94.7 ± 1.9	96.0 ± 0.0	88.0 ± 0.0	96.0 ± 0.0	100.0 ± 0.0	98.7 ± 1.9	91.7 ± 12.6
<b>Task Mean</b>	73.0 ± 1.6	52.6 ± 1.0	59.8 ± 0.8	62.7 ± 0.5	61.3 ± 1.0	62.4 ± 1.4	68.1 ± 1.6	69.7 ± 1.4	63.7 ± 6.1

Table 15. Success Rates of ARP under Different Perturbations of RL Bench-OG.

Task Name	Occlusion 1	Occlusion 2	Light Color	Table Color	Table Texture	Distractor	Background Texture	Camera Pose	Variant Mean
basketball_in_hoop	0.0 ± 0.0	0.0 ± 0.0	0.0 ± 0.0	0.0 ± 0.0	0.0 ± 0.0	0.0 ± 0.0	0.0 ± 0.0	0.0 ± 0.0	0.0 ± 0.0
scoop_with_spatula	0.0 ± 0.0	0.0 ± 0.0	0.0 ± 0.0	0.0 ± 0.0	0.0 ± 0.0	1.3 ± 1.9	1.3 ± 1.9	0.0 ± 0.0	0.3 ± 1.1
take_plate_off_colored_dish_rack	4.0 ± 0.0	0.0 ± 0.0	0.0 ± 0.0	0.0 ± 0.0	2.0 ± 2.0	0.0 ± 0.0	0.0 ± 0.0	0.0 ± 0.0	0.8 ± 1.6
water_plants	2.0 ± 2.0	4.0 ± 0.0	8.0 ± 0.0	4.0 ± 3.3	2.0 ± 2.0	8.0 ± 3.3	2.0 ± 2.0	2.0 ± 2.0	4.0 ± 3.3
block_pyramid	0.0 ± 0.0	0.0 ± 0.0	0.0 ± 0.0	0.0 ± 0.0	0.0 ± 0.0	0.0 ± 0.0	0.0 ± 0.0	0.0 ± 0.0	0.0 ± 0.0
solve_puzzle	0.0 ± 0.0	0.0 ± 0.0	0.0 ± 0.0	0.0 ± 0.0	0.0 ± 0.0	0.0 ± 0.0	0.0 ± 0.0	0.0 ± 0.0	0.0 ± 0.0
take_usb_out_of_computer	92.0 ± 8.0	82.0 ± 2.0	61.3 ± 3.8	58.7 ± 5.0	66.0 ± 2.0	76.0 ± 0.0	65.3 ± 7.5	64.0 ± 12.0	70.7 ± 12.5
close_drawer	76.0 ± 0.0	56.0 ± 8.0	86.7 ± 5.0	88.0 ± 3.3	72.0 ± 0.0	84.0 ± 3.3	92.0 ± 3.3	74.0 ± 2.0	78.6 ± 11.6
straighten_ropes	0.0 ± 0.0	0.0 ± 0.0	0.0 ± 0.0	0.0 ± 0.0	0.0 ± 0.0	0.0 ± 0.0	0.0 ± 0.0	0.0 ± 0.0	0.0 ± 0.0
toilet_seat_down	100.0 ± 0.0	92.0 ± 8.0	73.3 ± 5.0	74.7 ± 1.9	84.0 ± 4.0	74.7 ± 13.2	88.0 ± 8.6	82.0 ± 2.0	83.6 ± 11.1
<b>Task Mean</b>	27.4 ± 0.8	23.4 ± 1.1	22.9 ± 0.8	22.5 ± 0.7	22.6 ± 0.5	24.4 ± 1.4	24.9 ± 1.2	22.2 ± 1.2	23.8 ± 1.9

Table 16. Success Rates of Diffusion Policy under Different Perturbations of RL Bench-OG.

so on. TVVE is trained with 100 demonstrations per task. Example demonstration samples for each task are shown in Fig. 9. During evaluation, the model is tested with 25 demonstrations using the same settings. For a more intuitive understanding, we also include corresponding video results.

### RLBench-OG: Task Definition and Visualization.

RLBench-OG is derived from the RL Bench benchmark and is designed to evaluate the robustness of models under occlusion as well as their generalization capability under various environmental perturbations. RLBench-OG selects ten tasks from the original RL Bench task list, covering both simple scenarios (e.g., *take\_usb\_out\_of\_computer*) and more complex long-horizon tasks (e.g., *block\_pyramid*). The benchmark consists of two components: an **Occlusion Suite** and a **Generalization Suite**. We detail both components below. For the visualization of different variant settings corresponding to each task, see Fig. 12 and Fig. 13.

#### Occlusion Suite

Occlusion refers to situations in which the line of sight of the camera to key task-relevant regions is fully or partially blocked, leading to incomplete observations and degraded performance of state estimation and action execution. In the occlusion suite, we introduce occlusions to the *front\_camera* through two mechanisms:

1. **Self-occlusion by object pose perturbation.** We modify the position or orientation of task-relevant objects such that essential interaction points become occluded. These occluded regions are often critical for task com-

pletion, such as the drawer handle in the *close\_drawer* task.

2. **Occlusion by external distractors.** We place task-irrelevant objects—such as cabinets, TVs, or doors—in front of the workspace to partially block the scene, leading to incomplete visibility of key regions.

**Task Construction.** The following describes how occlusions are introduced for each of the ten tasks:

- **basketball\_in\_hoop:** Basket and trash can poses are perturbed to occlude the basketball.
- **block\_pyramid:** A cabinet is placed in front of the workspace to occlude part of the blocks.
- **close\_drawer:** The drawer is rotated such that its geometry occludes the handle.
- **scoop\_with\_spatula:** A wine bottle is positioned to block the target cube.
- **solve\_puzzle:** A storage cabinet is placed to occlude puzzle pieces.
- **straighten\_ropes:** A desk lamp is placed in front of one end of the rope.
- **take\_plate\_off\_colored\_dish\_rack:** A box with a laptop blocks visibility of the plate.
- **take\_usb\_out\_of\_computer:** A cabinet blocks the USB port area.
- **toilet\_seat\_down:** A door is placed such that it occludes the toilet seat.
- **water\_plants:** A television partially blocks both the watering can and the plant.

Avg. SR (%)	Seen																	Unseen			
	Insert onto Square Peg in Drawer	Put Item in Drawer	Reach and Drag	Turn Tap	Slide Block to Color Target	Open Drawer	Put Groceries in Cupboard	Place Shape in Shape Sorter	Put Money in Safe	Push Buttons	Close Jar	Stack Blocks	Place Cups	Place Wine at Rack Location	Light Bulb In	Sweep to Dustpan of Size	Meat off Grill	Stack Cups	Water Plants	Close Drawer	Toilet Seat Down
80.2	24.0	100.0	96.0	100.0	100.0	88.0	68.0	32.0	96.0	96.0	100.0	68.0	36.0	96.0	88.0	96.0	96.0	64.0	12.0	44.0	100.0

Table 17. **Performance with  $N_G = 8, N_E = 16$  TaskMoE in RL Bench.** TaskMoE enhances generalization to unseen tasks.

**Experimental Settings.** We evaluate models under two occlusion levels, **Occlusion 1** and **Occlusion 2**. For **Occlusion 1**, models are both trained and tested directly under the occluded task configurations; for **Occlusion 2**, models are trained in the original RL Bench task settings and then evaluated in a zero-shot manner under occluded conditions.

### Generalization Suite

The Generalization Suite evaluates robustness to environment-conditioned variations. Based on the same ten tasks, we construct six types of environment variations, each modifying exactly one factor while keeping all others unchanged. Following the pipeline from the COLOSSEUM [40], we specify variation types using *yaml* configuration files and data collection procedures via *json* metadata.

### Variation Types.

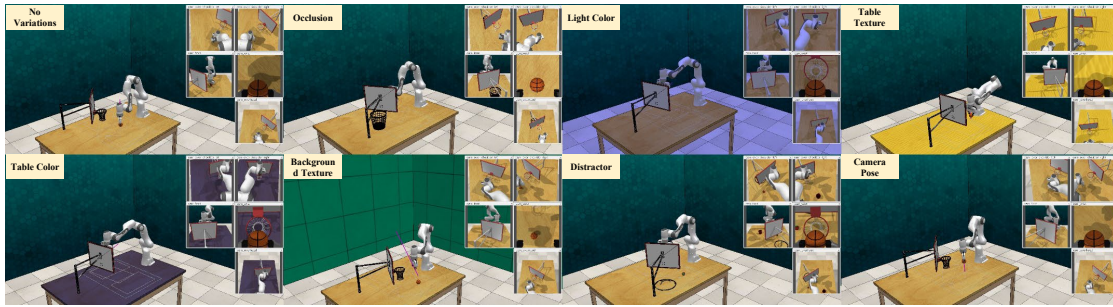
- **light\_color:** RGB values are sampled within predefined ranges and applied to directional lights.
- **table\_texture:** A texture is sampled from a texture dataset and applied to the table.
- **table\_color:** RGB values are sampled within predefined ranges and applied to the table surface.
- **background\_texture:** A background texture is randomly sampled and applied.
- **distractor:** Two distractor objects are sampled from a 3D asset dataset and spawned within the workspace boundary.
- **camera\_pose:** Camera position and orientation offsets are sampled and applied to the front, left-shoulder, and right-shoulder cameras.

**Experimental Settings.** For the Generalization Suite, models are trained in the original RL Bench environment and subsequently evaluated in a zero-shot manner across various generalization variants. For all variants, we collect 25 validation episodes for each task.

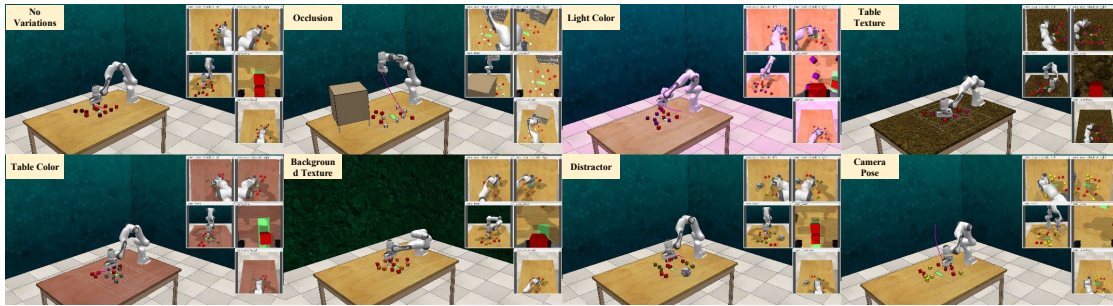
## Appendix E. Multi-view Re-rendering Visualization Results

To further illustrate the operational principles of our TVVE framework and its performance on RL Bench, we visualize multiple dynamic virtual viewpoints generated by MVEP in 3D space at intermediate execution steps during inference, along with their corresponding rendered 2D images for each scene, as shown in Fig. 14 and Fig. 15. The rendered imagery clearly captures both the end-effector and target ob-

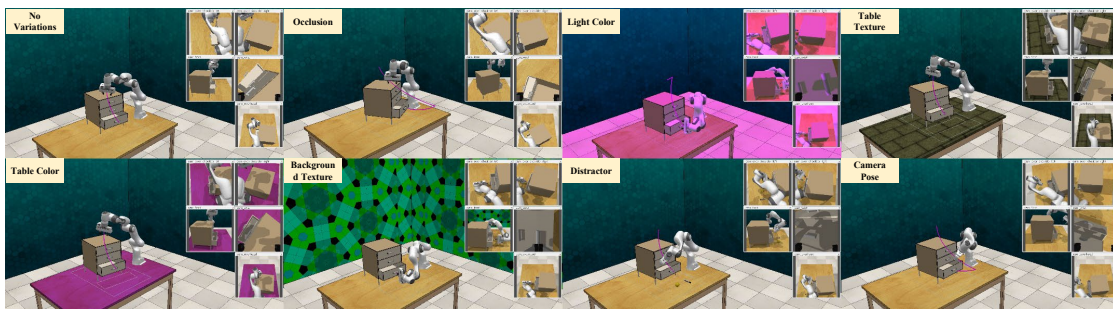
jects, enabling the action model to make more precise motion predictions based on these perceptual cues. This enhancement directly contributes to improved task success rates across multiple manipulation scenarios. TVVE effectively translates visual completeness into manipulation success, validating that dynamic “seeing” fundamentally underpins robust “acting.”



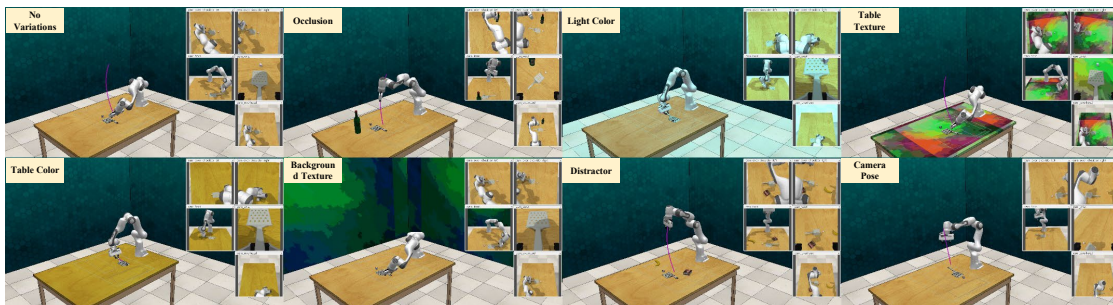
(a) Basketball In Hoop: pick up the basketball and put it in the hoop.



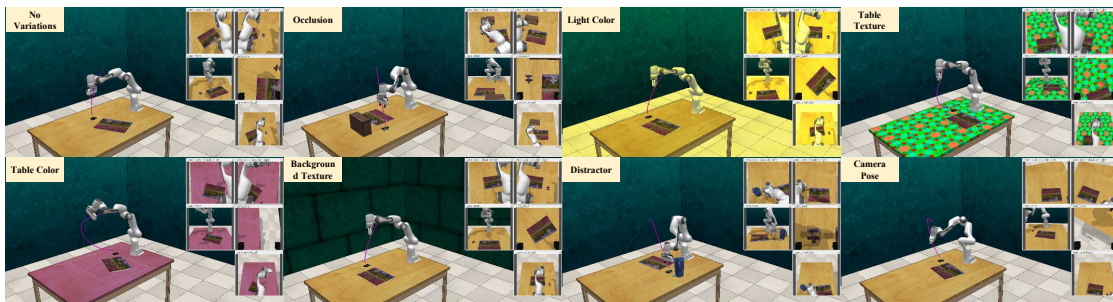
(b) Block Pyramid: stack red blocks in a pyramid.



(c) Close Drawer: close of the bottom drawer by pushing it shut.

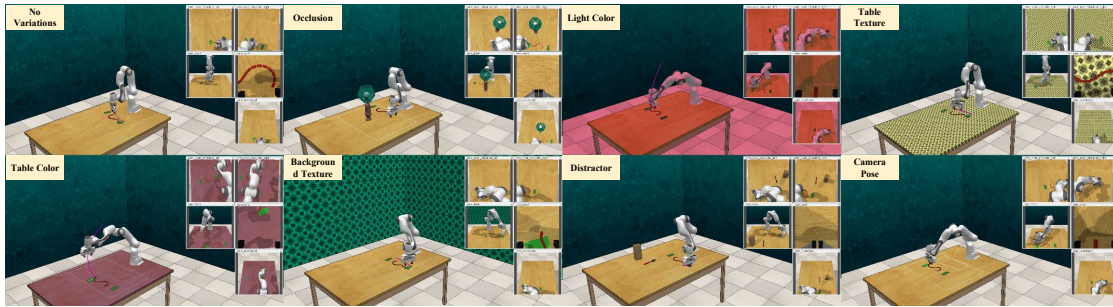


(d) Scoop With Spatula: scoop up the cube and lift it with the spatula.

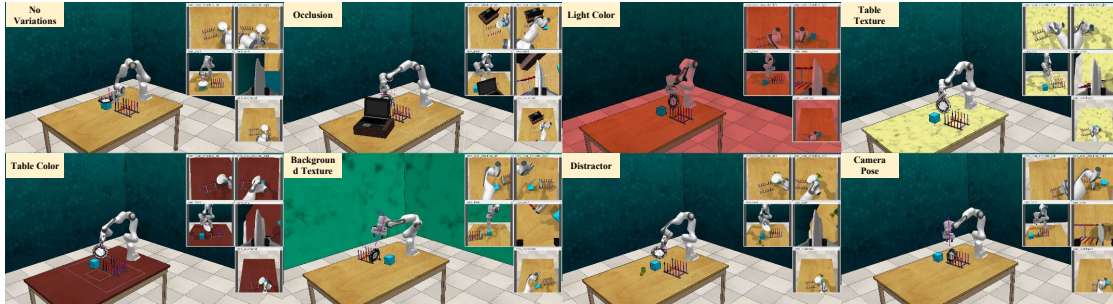


(e) Solve Puzzle: pick up the puzzle piece and place it on the puzzle.

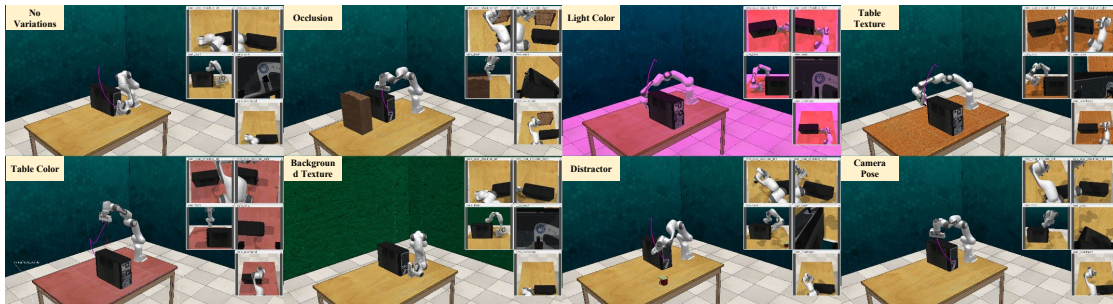
Figure 12. Visualization of different variants for the **basketball\_in\_hoop**, **block\_pyramid**, **close\_drawer**, **scoop\_with\_spatula**, **solve\_puzzle** tasks.



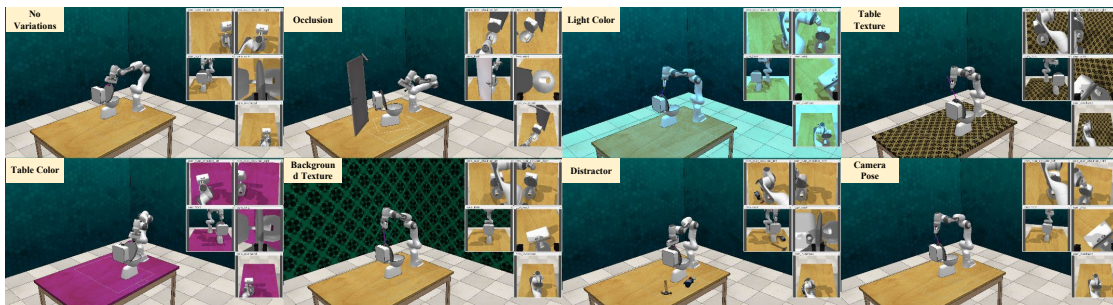
(f) Straighten Rope: grasping each end of the rope in turn, leave the rope straight.



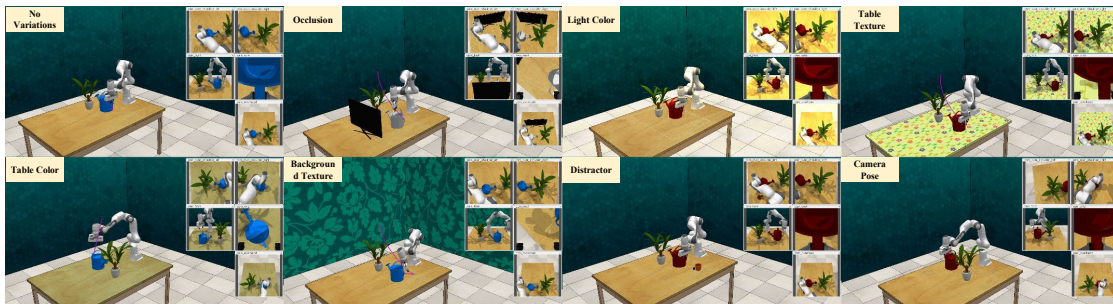
(g) Take Plate Off Colored Dish Rack: remove the dish from the black rack.



(h) Take Usb Out Of Computer: grasp the usb stick and slide it out of the pc.



(i) Toilet Seat Down: grasping the top of the lid, close the toilet seat.



(j) Water Plants: pick up the watering can by its handle and water the plant.

Figure 13. Visualization of different variants for the `straighten_rope`, `take_plate_off_colored_dish_rack`, `take_usb_out_of_computer`, `toilet_seat_down`, `water_plants` tasks.

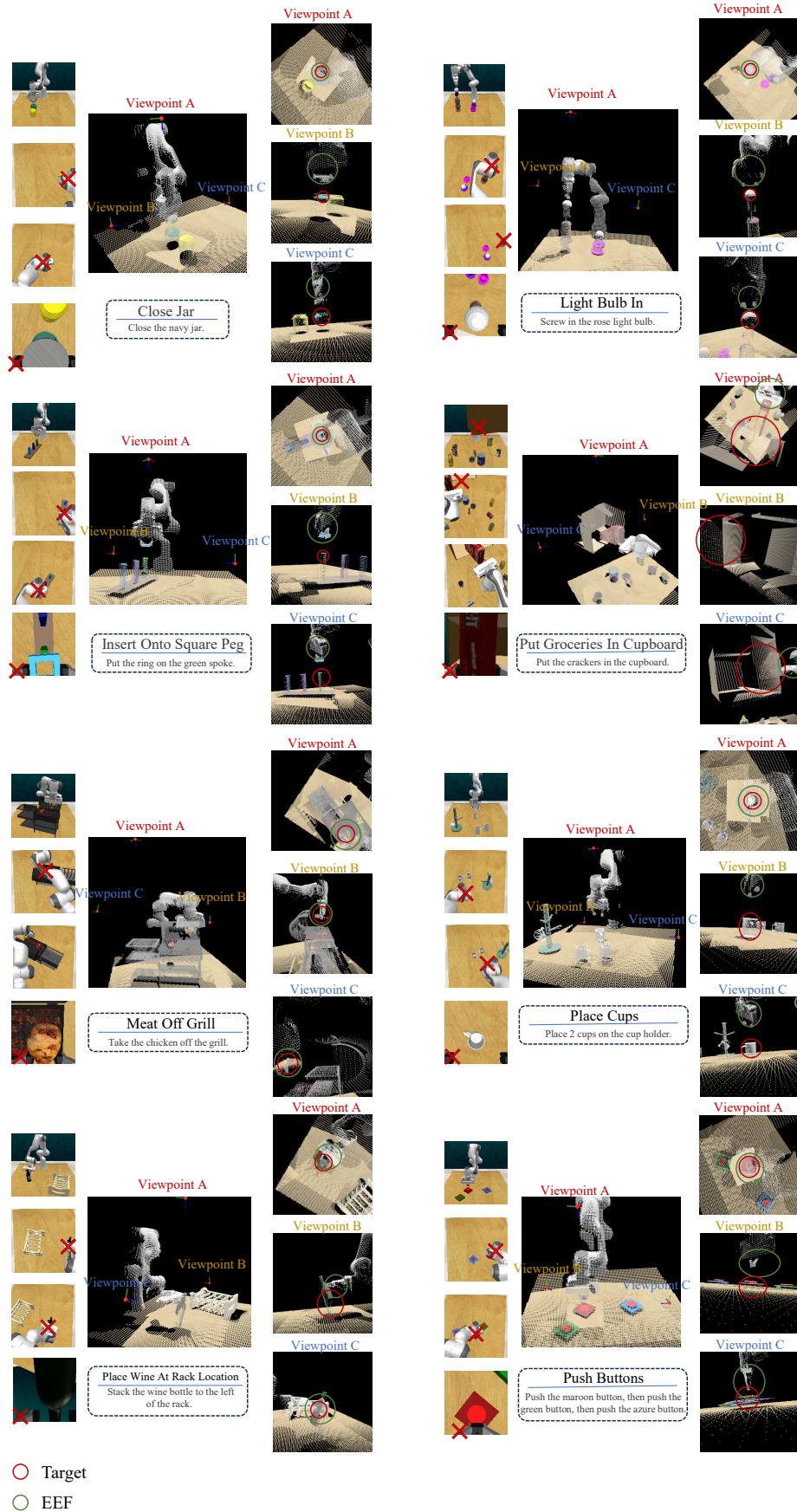


Figure 14. The dynamic multi-view re-rendering visualization results of the **Light Bulb In**, **Close Jar**, **Insert Onto Square Peg**, **Put Groceries In Cupboard**, **Grill**, **Place Cups**, **Place Wine At Rack Location**, and **Push Buttons** tasks.



Figure 15. The dynamic multi-view re-rendering visualization results of the **Put Item In Drawer**, **Put Money In Safe**, **Reach And Drag**, **Slide Block To Color Target**, **Stack Blocks**, **Stack Cups**, **Sweep To Dustpan Of Size**, and **Turn Tap** tasks.